



**Universidade do Minho**  
Escola de Engenharia??  
Departamento de Informática??

Jaime Santos

**Staggered Quantum Walks in Qiskit??**  
**Second Part of Title**

**First Part of Subtitle**  
**Second part of Subtitle**

April 2021



**Universidade do Minho**

Escola de Engenharia??

Departamento de Informática??

Jaime Santos

**Staggered Quantum Walks in Qiskit??**  
**Second Part of Title**

**First Part of Subtitle**

**Second part of Subtitle**

Master dissertation

Master Degree in Física da Informação

Dissertation supervised by

**Luís Barbosa**

**Bruno Chagas**

April 2021

---

## ACKNOWLEDGEMENTS

---

Write acknowledgements here

---

## ABSTRACT

---

Implementation of staggered quantum walks in qiskit.

---

## RESUMO

---

Pensar no que escrever aqui. Hello!

---

## CONTENTS

---

1	INTRODUCTION	1
1.1	Brief history of quantum computing	1
1.2	Classical and Quantum Random Walks	4
1.3	State of the Art quantum walks implementations	4
1.4	Text overview and contributions	4
2	QUANTUM COMPUTING	5
2.1	Grover's Algorithm	5
2.1.1	One marked element	7
2.1.2	Multiple marked elements	9
2.1.3	Single-Shot Grover	10
2.2	Quantum Fourier Transform	11
3	QUANTUM WALKS	14
3.1	Classical Random Walk	14
3.2	Coined Quantum Walk	15
3.3	Continuous-Time Quantum Walk	20
3.4	Staggered Quantum Walk	25
3.5	Search problems with Quantum Walks	27
3.5.1	Coined	28
3.5.2	Staggered	29
3.5.3	Continuous	31
4	IMPLEMENTATIONS AND APPLICATIONS	35
4.1	Coined	35
4.2	Continuous	40
4.3	Staggered	44
4.4	Search Problems with Qiskit	44
4.4.1	Grover	44
4.4.2	Coined	46
4.4.3	Continuous	48
4.4.4	Staggered	51
5	DISCUSSIONS AND CONCLUSION	52
5.1	Conclusions	52
5.2	Prospect for future work	52

A SUPPORT MATERIAL

57

---

## LIST OF FIGURES

---

Figure 1	Grover one marked element temp.	8
Figure 2	Grover Multiple marked temp.	9
Figure 3	Single Shot temp	10
Figure 4	Temp	12
Figure 5	Classical Walk Temp.	14
Figure 6	Probability distribution for the coined quantum walk on a line, after 100 steps, with initial condition $ \Psi(0)\rangle =  0\rangle  x=0\rangle$ and the Hadamard coin.	18
Figure 7	Probability distribution for the coined quantum walk on a line, after 100 steps, with initial condition $ \Psi(0)\rangle = - 1\rangle  x=0\rangle$ and the Hadamard coin.	18
Figure 8	Probability distribution for the coined quantum walk on a line, after 100 steps, with initial condition $ \Psi(0)\rangle = \frac{ 0\rangle - i 1\rangle}{\sqrt{2}}  x=0\rangle$ and the Hadamard coin.	19
Figure 9	Probability distribution for the continuous-time quantum walk on a line, at $t = 100$ , with initial condition $ \Psi(0)\rangle =  0\rangle$ and $\gamma = \frac{1}{2\sqrt{2}}$ .	22
Figure 10	Probability distribution for the continuous-time quantum walk on a line, after 100 steps, with initial condition $ \Psi(0)\rangle =  0\rangle$ and $\gamma = \frac{1}{6\sqrt{2}}$ .	23
Figure 11	Temporary	23
Figure 12	Probability distribution for the continuous-time quantum walk on a line, after 100 steps, with initial condition $ \Psi(0)\rangle = \frac{ 0\rangle +  1\rangle}{\sqrt{2}}$ and $\gamma = \frac{1}{2\sqrt{2}}$ .	24
Figure 13	Temporary	24
Figure 14	Probability distribution for the staggered quantum walk on a line after 50 steps, with initial condition $ \Psi(0)\rangle = \frac{ 0\rangle +  1\rangle}{\sqrt{2}}$ , for multiple angles.	27
Figure 15	$ \Psi(0)\rangle =  0\rangle$	27
Figure 16	$ \Psi(0)\rangle =  1\rangle$	27
Figure 17	Discrete-time coined quantum walk search for a complete graph with 16, 32 and 64 nodes.	30



Figure 18	Maximum probability of the marked element as a function of the $\theta$ value plotted from 0 to $\pi$ for number of nodes $N = 64, 128$ and 256.	31
Figure 19	Staggered quantum walk search for a complete graph with 16, 32 and 64 nodes.	32
Figure 20	Value of the difference between the largest eigenvalue and the second largest, plotted as a function of $\gamma N$ , for $N = 512$ .	33
Figure 21	Continuous quantum walk search for a complete graph with 16, 32 and 64 vertices.	34
Figure 22	Douglas wang shift operator	36
Figure 23	Douglas wang coined quantum walk circuit	36
Figure 24	Toffoli decomposition	36
Figure 25	General decomposition	37
Figure 26	Temp	38
Figure 27	Temp	38
Figure 28	Temp	39
Figure 29	Temp	39
Figure 30	Temp	42
Figure 31	Temp	42
Figure 32	temp	42
Figure 33	Temp	43
Figure 34	Temp	43
Figure 35	Temp	45
Figure 36	Temp	45
Figure 37	Temp	45
Figure 38	Temp	46
Figure 39	Douglas wang coined quantum walk circuit	47
Figure 40	Temp	47
Figure 41	Temp	47
Figure 42	Temp	48
Figure 43	Temp	48
Figure 44	Temp	49
Figure 45	Temp	50
Figure 46	Temp	50
Figure 47	Temp	50
Figure 48	Temp	50
Figure 49	Temp	51

---

## LIST OF TABLES

---

---

## INTRODUCTION

---

### 1.1 BRIEF HISTORY OF QUANTUM COMPUTING

The modern understanding of computer science was firstly announced by [Turing \(1936\)](#) where he developed the abstract concept of what is now called a *Turing machine*. These machines are the mathematical foundation of programmable computers, and Turing showed that there is a *Universal Turing Machine* that can be used to simulate any other Turing Machine. This means that if an algorithm can be executed in any piece of hardware, then there is a Universal Turing Machine that can accomplish the same task. This is known as the *Church-Turing thesis*, which connects the concept of what classes of algorithms can be run in some physical device with the mathematical framework of a Universal Turing Machine.

The paper published by Turing set in motion a series of events which led to the rapid advancement of electronic computers and computer science. One of the earliest theoretical models developed by John von Neumann (work later published in [von Neumann \(1993\)](#)), presented how to assemble all the necessary parts to create a computer with all the capabilities of a Universal Turing Machine. The true explosion of innovation in this field came after the invention of the transistor in 1947 by John Bardeen and Walter Brattain. The creation of the transistor led to an unprecedented growth quantified by [Moore \(1965\)](#) where he created *Moore's law*, stating that computer power will double with constant cost approximately every two years. Moore's law has roughly held true throughout the decades, by the ever increasing miniaturization of the transistor technology. However, conventional fabrication methods run into a problem of scale, as quantum effects begin to interfere more as the size of the devices becomes smaller.

[Feynman \(1959\)](#) recognized such a miniaturization was the way forward, and even predicted the problems quantum effects presented to a classical computer. With an amazing stroke of insight, Feynman imagined that these effects could be exploited given the right computational paradigm. Quantum computing begins to take form in later work developed by [Benioff \(1980\)](#), where the earliest quantum mechanical model of a computer was described. In this paper, Benioff showed that a computer working under the laws of quantum mechanics could be used to express a Schrödinger equation description of Turing machines. Shortly

after, Feynman (1982) pointed out that simulating quantum systems on classical computers is inefficient, and suggested using quantum computers for this purpose. Additional work in the following decade further explored this idea and showed that there are systems that quantum computers can simulate, which have no known efficient simulation on a classical computer, and even today this continues to be one of the most promising fields in quantum computing.

Driven by the work of Turing, Deutsch (1985) questioned if a stronger version of the Church-Turing thesis could be derived from the laws of physics. The strong Church-Turing thesis states that any algorithmic process can be simulated efficiently using a probabilistic Turing machine, and Deutsch was set to define some device that could efficiently simulate an arbitrary physical system. Whether Deutsch's formulation of a Universal Quantum Computer is sufficient for this function is still an open question, but what he accomplished was a challenge to the strong Church-Turing thesis by suggesting that there are tasks a quantum computer can accomplish efficiently that a probabilistic Turing machine cannot. Deutsch and Jozsa (1992) present an example of a quantum algorithm that is exponentially faster than a classical counterpart, the *Deutsch-Jozsa algorithm* that determines if a function is constant or balanced. Even though of little practical use, this is one of the first examples of possible advantages a quantum computer may have over a classical one.

Even though the Deutsch-Jozsa algorithm might not have real world applications, it led to further research on finding other such types of algorithms. Shor (1994a) showed that the problem of finding prime factors of an integer and the *discrete logarithm* problem can be efficiently solved by a quantum computer by an exponential factor. This brought a lot of interest to quantum computing, since both of these problems have real world applications and no efficient classical solution was/is known. Furthermore, most modern popular algorithms used for cryptography rely on the fact that the integer factorization or discrete logarithm problems are not efficiently solved. Since this is no longer the case, a new field has emerged called *Post-quantum cryptography*, whose purpose is to find suitable classical algorithms for cryptography that are not efficiently solved by quantum computing.

A more modest, but very relevant advantage was presented by Grover (1996) where he presented a quantum algorithm that promised to speed up unstructured database searches quadratically. Even though it's not an exponential improvement like Shor's algorithm, search-based algorithms are useful in many contexts, so even a "small" quadratic gain generated a lot of interest.

Contemporary to computer science, information theory is another field very relevant to this topic. Shannon (1948) revolutionized how communication and information are understood. In his paper, Shannon was interested in defining what resources are required to send information over a communication channel and how to reliably send that information mitigating the effects of noise. This led to the creation of the two fundamental theorems

of information theory. Firstly, Shannon's *noiseless channel coding theorem*, specifies what resources are needed to store information sent from a source. Secondly, the *noisy channel coding theorem*, specifies how much information can be sent through a channel subject to noise. Even though Shannon's second theorem does not define any specific methodology to reduce noise, it sets an upper limit on how much noise can be mitigated through said methodology. These are known as *error-correcting codes* and research has developed better and better codes that get closer and closer to Shannon's limit, and they are used wherever there is need to store or transmit information.

Similar progress was made in quantum information theory. Schumacher (1995) developed a quantum version of Shannon's noiseless coding theorem, where he defined a *quantum bit* as a physical resource. There is no analogue for the second Shannon theorem, but that didn't stop the development of quantum error-correcting theory. For example, Calderbank and Shor (1996) and Steane (1996) proposed an important class of quantum error-correcting codes known as CSS.

Error-correcting was designed to protect quantum states, but another discovery by Bennett and Wiesner (1992) showed another interesting aspect about quantum information when transmitting classical information through a quantum channel. They explained how to send two classical bits of information using only one qubit, in a phenomenon known as *superdense coding*.

Another interesting application of quantum information is in the field of cryptography. Wiesner (1983) showed how quantum mechanics could be used to make sure that a information sent could not be interfered with without destroying it. Building on this work, Bennett and Brassard (1984) proposed a quantum key distribution protocol between sender and receiver that could not be spied upon without notice. Many other protocols have since been proposed and experimental prototypes developed.

Finally, another interesting field within quantum computation is based on the concept of *distributed quantum computation*. Quantum clusters show promise since they require exponentially less communication to solve certain problems, such as modeling quantum systems, but are still in their infancy due to technical restrictions. There has been increasing international interest in taking advantage of these systems to build a *quantum internet* which promises better and safer transmission of information, but there are still many technological improvements to be made before this replaces current internet.

1.2 CLASSICAL AND QUANTUM RANDOM WALKS

1.3 STATE OF THE ART QUANTUM WALKS IMPLEMENTATIONS

1.4 TEXT OVERVIEW AND CONTRIBUTIONS

---

## QUANTUM COMPUTING

---

### 2.1 GROVER'S ALGORITHM

Searching through an unstructured database is a task classically achieved by exhaustively evaluating every element in the database. Assume there exists a black box (oracle) that can be asked to find out if two elements are equal. Since we're looking for a specific element in a database of size  $N$ , we'd have to query the oracle on average  $\frac{N}{2}$  times, or in the worst case  $N$  times.

Grover's algorithm, presented in [Grover \(1996\)](#), comes as a quantum alternative to this type of problems, taking advantage of superposition by increasing desirable states' amplitudes through a process called *amplitude amplification*. This method has a quadratic gain over the classical counterpart [Boyer et al. \(1998\)](#), being able to find a target element in expected time  $\mathcal{O}(\sqrt{N})$ .

Let us now expand on the inner workings of the black box. We start by focusing on searching indexes instead of directly evaluating the element and we assume  $N = 2^n$ ,  $n$  being a positive integer. We can now define a function  $f : \{0, 1, \dots, N - 1\}$  that returns 1 when evaluating the desired (marked) element and 0 otherwise. Since this function is to be applied to a quantum system, we must build a unitary operator  $\mathcal{O}$

$$\mathcal{O} |x\rangle |i\rangle = |x\rangle |i \oplus f(x)\rangle. \quad (1)$$

where  $|x\rangle$  is the index register,  $\oplus$  is the binary sum operation and  $|i\rangle$  is a qubit that is flipped if  $f(x) = 1$ .

The action of the oracle on state  $|0\rangle$  will be

$$\mathcal{O} |x\rangle |0\rangle = \begin{cases} |x_0\rangle |1\rangle, & \text{if } x = x_0 \\ |x\rangle |0\rangle, & \text{otherwise.} \end{cases} \quad (2)$$

where  $x_0$  is the marked element. More generically,  $\mathcal{O}$  can be written as

$$\mathcal{O} |x\rangle = (-1)^{f(x)} |x\rangle. \quad (3)$$

This offers a bit of insight into the oracle, it *marks* the solutions to the search problem by applying a phase shift to the solutions. The question now is, what is the procedure that determines a solution  $x_0$  using  $\mathcal{O}$  the minimum number of times? The answer lies in the amplitude amplification section of Grover's search, starting with the creation of a uniform superposition

$$|\Psi_0\rangle = H^{\otimes n} |x\rangle = \frac{1}{\sqrt{N}} \sum_{x=0}^{N-1} |x\rangle \quad (4)$$

where  $H^{\otimes n}$  is the *Hadamard* operator applied to an arbitrary number of states.

If we were to measure  $|x\rangle$  at this point, the superposition would collapse to any of the base states with the same probability  $\frac{1}{N} = \frac{1}{2^n}$ , which means that on average, we'd need to try  $N = 2^n$  times to guess the correct item. This is where amplitude amplification comes into effect, by means of a second unitary operator

$$\mathcal{D} = (2|\Psi_0\rangle\langle\Psi_0| - I) = H^{\otimes n}(2|0\rangle\langle 0| - I)H^{\otimes n} \quad (5)$$

This operator applies a conditional phase shift, with every computational basis state except  $|0\rangle$  receiving a phase shift. This can also be described as the *inversion about the mean*, for a state of arbitrary amplitudes

$$|\phi\rangle = \sum_{k=0}^{N-1} \alpha_k |k\rangle \quad (6)$$

the action of  $\mathcal{D}$  on state  $\phi$  will be

$$\mathcal{D}|\phi\rangle = \sum_{k=0}^{N-1} (-\alpha_k + 2\langle\alpha\rangle) |k\rangle \quad (7)$$

where  $\langle\alpha\rangle$  is the average of  $\alpha_k$

$$\langle\alpha\rangle = \frac{1}{N} \sum_{k=0}^{N-1} \alpha_k |k\rangle \quad (8)$$

The evolution operator that performs one step of the algorithm is then

$$\mathcal{U} = \mathcal{D}\mathcal{O} \quad (9)$$

and after  $t$  steps the state of the system is

$$|\Psi(t)\rangle = \mathcal{U}^t |\Psi_0\rangle. \quad (10)$$



## 2.1.1 One marked element

The optimal number of steps is, as aforementioned, proportional to  $\sqrt{N}$ . More precisely, if there's only one solution, maximum probability can be reached in *approximately*  $\frac{\pi}{4}\sqrt{N}$  iterations. In order to show that this is the case, an iteration will be formally defined here as the process that transforms the state

$$|\Psi(k, l)\rangle = k|i_0\rangle + \sum_{i \neq i_0} l|i\rangle \quad (11)$$

into state  $|\Psi(\frac{N-2}{N}k + \frac{2(N-1)}{N}l, \frac{N-2}{N}l - \frac{2}{N}k)\rangle$ . Amplitudes  $l$  and  $k$  are real numbers that satisfy  $k^2 + (N-1)l^2 = 1$ . Running  $m$  iterations over state  $|\Psi_0\rangle$  will eventually lead to state  $|\Psi_j\rangle = |\Psi(k_j, l_j)\rangle$  after the  $j$ -th iteration, where  $k_0 = l_0 = \frac{1}{\sqrt{N}}$  and

$$\begin{cases} k_{j+1} = \frac{N-2}{N}k_j + \frac{2(N-1)}{N}l_j \\ l_{j+1} = \frac{N-2}{N}l_j + \frac{2}{N}k_j. \end{cases} \quad (12)$$

After the last iteration, the system will be in state  $|\Psi_m\rangle$  with a certain amplitude. If that amplitude corresponds to the marked element  $x_0$ , then it is said that the algorithm was successful.

Grover (1996) proves that there exists a value of  $m < \sqrt{2N}$  such that the probability of success is at least  $\frac{1}{2}$ . However the probability of success does not linearly increase with the number of iterations, in fact for  $m = \sqrt{2N}$  the system will succeed less than 1 in 10 times. Boyer et al. (1998) argues that an explicit value of  $m$  is needed, and it is achieved by finding a closed form formula for  $k_j$  and  $l_j$ . The first step is to define an angle  $\theta$  so that  $\sin^2 \theta = \frac{1}{N}$ , and equation 12 will become

$$\begin{cases} k_{j+1} = \sin((2j+1)\theta) \\ l_{j+1} = \frac{1}{\sqrt{N-1}} \cos((2j+1)\theta). \end{cases} \quad (13)$$

In order to maximize the probability of success, one must find a value of  $m$  so that  $k_m = 1$  and  $l_m$  is as close to 0 as possible. The value of  $k$  after  $m$  iterations will be at its maximum when  $\sin((2m+1)\theta) = \frac{\pi}{2}$ , and solving the trigonometric equation leads to a value of  $m = \frac{\pi-2\theta}{4\theta}$ . Conversely,  $l_{\tilde{m}} = 0$  when  $\tilde{m} = \frac{\pi-2\theta}{4\theta}$  for an integer number of  $\tilde{m}$ . Setting  $m$  to the nearest lower integer of  $\frac{\pi}{4\theta}$  will lead to

$$|m - \tilde{m}| \leq \frac{1}{2} \iff |(2m+1)\theta - (2\tilde{m}-1)\theta| \leq \frac{\pi}{2}. \quad (14)$$

By definition,  $(2\tilde{m} + 1)\theta = \frac{\pi}{2}$  which means that  $|\cos((2m + 1)\theta)| \leq |\sin \theta|$ . The probability of failure after  $m$  iterations can then be written as

$$(N - 1)l_m^2 = \cos^2((2m + 1)\theta) \leq \sin^2 \theta = \frac{1}{N}. \quad (15)$$

Failure decreases as the number of elements increases. The run time of the algorithm will be

$$m \leq \frac{\pi}{4\theta} \leq \frac{\pi}{4}\sqrt{N} \quad (16)$$

since  $\theta \geq \sin \theta = \frac{1}{\sqrt{N}}$ . This means that, for a large  $N$ , the number of iterations that maximizes the probability of success will be very close to  $\frac{\pi}{4}\sqrt{N}$ .

Figure 1 was obtained by coding the appropriate operators as to simulate the system presented in equation 10. The unitary evolution operator was applied approximately

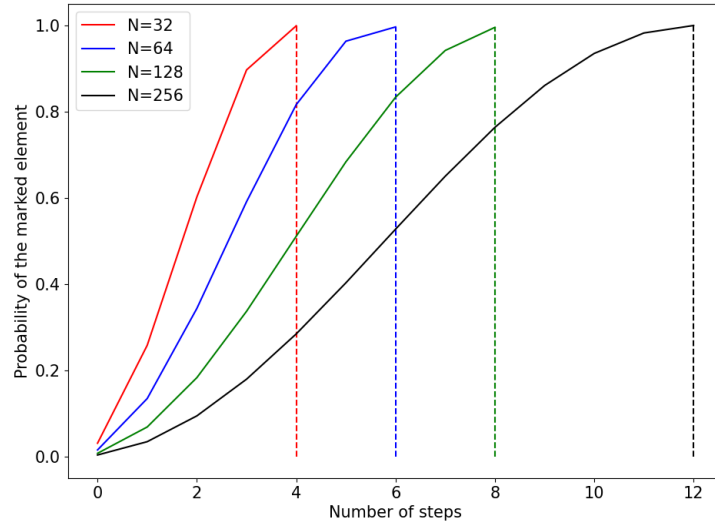


Figure 1: Grover one marked element temp.

$\frac{\pi}{4}\sqrt{N}$  times and the amplitudes associated with those states were stored as a probability distribution. Filtering the probability of the marked element and plotting it against the number of steps, shows that the maximum is indeed reached after the said number of iterations. It also shows that the maximum probability for  $N = 16$  is lower than for  $N = 128$ , which makes sense since the the probability of success is maximized for larger values of  $N$ .

### 2.1.2 Multiple marked elements

When there's more than one element marked by the oracle, the number of iterations to achieve maximum probability changes. In fact, the latter part of this section will be used to discuss the case where one single iteration of this algorithm is enough to achieve maximum probability.

Firstly, one must define a set  $A$  that is composed of all the marked elements and set  $B$  of the remaining. The state from equation 11 will become

$$|\Psi(k, l)\rangle = \sum_{i \in A} k |i\rangle + \sum_{x \in B} l |x\rangle. \quad (17)$$

Assuming  $t$  marked elements, iterating over this state will result in

$$\left| \Psi\left(\frac{N-2t}{N}k + \frac{2(N-1)}{N}l, \frac{N-2}{N}l - \frac{2}{N}k\right) \right\rangle. \quad (18)$$

Choosing an angle  $\theta$  such that  $\sin^2\theta = \frac{t}{N}$ , allows the definition of the amplitudes associated with the states after  $j$  iterations

$$\begin{cases} k_j = \frac{1}{\sqrt{t}} \sin((2j+1)\theta) \\ l_j = \frac{1}{\sqrt{N-t}} \cos((2j+1)\theta). \end{cases} \quad (19)$$

Similarly to the one solution case, it can be shown that setting the number of iterations

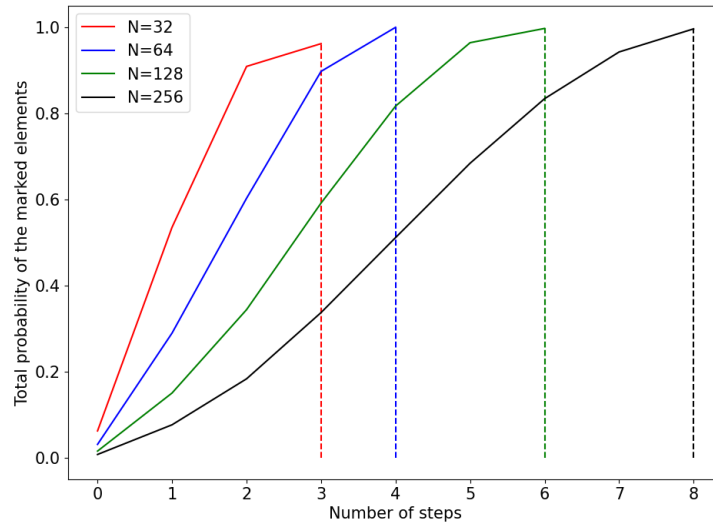


Figure 2: Grover Multiple marked temp.

$m$ , to the nearest lower integer of  $\frac{\pi}{4\theta}$  will result in a probability of failure  $(N - t)l_m^2 \leq \frac{t}{N}$ . Because  $\theta \geq \sin \theta = \sqrt{\frac{t}{N}}$  then

$$m \leq \frac{\pi}{4\theta} \leq \frac{\pi}{4} \sqrt{\frac{N}{t}}. \quad (20)$$

From a more practical perspective, if one were to mark two elements of a 64 element set, maximum probability is expected to be reached in approximately 4 steps, since  $\lfloor \frac{\pi}{4} \sqrt{\frac{64}{2}} \rfloor = 4$ . Likewise, for  $N = 256$ , the number of iterations is rounded to 8, which is plotted along several other values of  $N$  in figure 2. The y-axis is now the sum total probability of the marked elements and the x-axis represents the range of steps that spans from 0 to  $\lfloor \frac{\pi}{4} \sqrt{\frac{N}{2}} \rfloor$  for each  $N$ . Again, the probability of success approaches 1 as  $N$  increases. However, comparing to figure 1, the number of iterations that maximize probability is lower for each  $N$ , in agreement with equation 20.

### 2.1.3 Single-Shot Grover

An interesting case arises when the number of marked elements is set to  $t = \frac{N}{4}$ , because

$$\sin^2 \theta = \frac{\frac{N}{4}}{N} = \frac{1}{4} \iff \sin \theta = \frac{1}{2} \iff \theta = \frac{\pi}{6}. \quad (21)$$

Note that there are an infinite number of negative and positive solutions, but equation 21

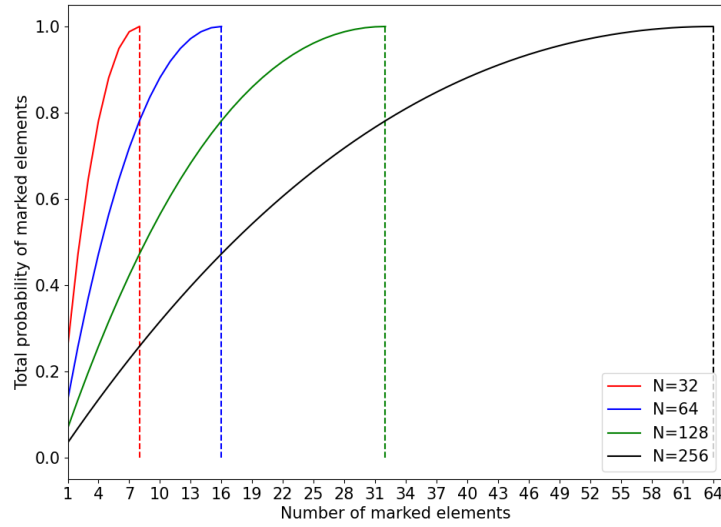


Figure 3: Single Shot temp

reflects the only relevant one in this context. As a consequence, amplitudes associated with state  $|\Psi(k_1, l_1)\rangle$  become

$$\begin{cases} k_1 = \frac{1}{\sqrt{t}} \sin((2+1)\theta) = \frac{1}{\sqrt{\frac{N}{4}}} \sin(3\frac{\pi}{6}) = \frac{2}{\sqrt{N}} \\ l_1 = \frac{1}{\sqrt{N-t}} \cos((2+1)\theta) = \frac{1}{\sqrt{N-\frac{N}{4}}} \cos(3\frac{\pi}{6}) = 0. \end{cases} \quad (22)$$

These results show that the amplitudes associated with the marked states double in relation to  $|\Psi_0\rangle$  and the remaining states disappear after only one iteration. This behaviour can be seen in figure 3, where the total probability of marked elements reaches 1 once the number of marked elements is  $\frac{1}{4}$  of the total elements.

## 2.2 QUANTUM FOURIER TRANSFORM

As was seen in section 2.1, quantum computers can perform certain tasks more efficiently than classical computers. Another such example is the problem of finding the prime factorization of an  $n$ -bit integer, which the most efficient solution to date, proposed by Pollard et al. (1994), requires  $e^{O(n^{\frac{1}{3}} \log^{\frac{2}{3}} n)}$  operations. In contrast, a quantum algorithm proposed by Shor (1994b) accomplishes the same task in  $O((\log n)^2 (\log \log n) (\log \log \log n))$  operations, which is an exponential gain due to the efficiency of the quantum Fourier transform.

The quantum Fourier transform is an implementation of the discrete Fourier transform over amplitudes of quantum states. It offers no speed ups when used in computing Fourier transforms of classical data, since the amplitudes cannot be accessed directly by measurement. Moreover, there is no known generalized efficient way of preparing the initial state to be Fourier Transform. What this means is that the uses of the QFT are not in the straightforward way of calculating discrete Fourier transforms, but in the form of algorithms, such as *phase estimation*, that take advantage of its properties. This transform can be described as the following operation over an orthonormal basis  $|0\rangle, |1\rangle, \dots, |N-1\rangle$

$$QFT(|j\rangle) = \frac{1}{\sqrt{N}} \sum_{k=0}^{N-1} e^{\frac{2\pi i j k}{N}} |k\rangle, \quad (23)$$

where  $N = 2^n$ . With a little bit of algebra, this can be rewritten as a product

$$\begin{aligned}
 \frac{1}{\sqrt{N}} \sum_{k=0}^{N-1} e^{\frac{2\pi ijk}{2^n}} |k\rangle &= \frac{1}{\sqrt{N}} \sum_{k_1=0}^1 \cdots \sum_{k_n=0}^1 e^{2\pi i j (\sum_{l=1}^n k_l 2^{-l})} |k_1 \cdots k_n\rangle \\
 &= \frac{1}{\sqrt{N}} \sum_{k_1=0}^1 \cdots \sum_{k_n=0}^1 \prod_{l=1}^n e^{2\pi i j k_l 2^{-l}} |k_l\rangle \\
 &= \frac{1}{\sqrt{N}} \bigotimes_{l=1}^n \left( \sum_{k_l=0}^1 e^{2\pi i j k_l 2^{-l}} |k_l\rangle \right) \\
 &= \frac{1}{\sqrt{N}} \bigotimes_{l=1}^n (|0\rangle + e^{2\pi i j 2^{-l}} |1\rangle)
 \end{aligned} \tag{24}$$

$$QFT(|x_1, \dots, x_n\rangle) = \frac{(|0\rangle + e^{2\pi i 0.x_n} |1\rangle)(|0\rangle + e^{2\pi i 0.x_{n-1}x_n} |1\rangle) \cdots (|0\rangle + e^{2\pi i 0.x_1x_2 \cdots x_n} |1\rangle)}{2^{\frac{N}{2}}}, \tag{25}$$

where  $x = x_1 2^{n-1} + x_2 2^{n-2} + \cdots + x_n 2^0$  and the notation  $0.x_1 x_{l+1} \cdots x_n$  represents the binary fraction  $\frac{x_l}{2^{l^0}} + \frac{x_{l+1}}{2^1} \cdots \frac{x_m}{2^{m-l+1}}$ . This is a very useful representation because it makes constructing an efficient circuit much simpler, as can be seen in figure 4. However, the circuit implementation of the QFT requires exponentially smaller phase-shift gates as the number of qubits increases. This can be somewhat mitigated by eliminating the smaller phase-shift gates at the cost of some accuracy, as was shown in [Coppersmith \(1994\)](#) where he defined the *approximate* quantum Fourier transform. This approximation requires only  $O(n \log n)$  gates, and work by [Barenco et al. \(1996\)](#) and [Cheung \(2004\)](#) established lower bounds for the probability of the approximate state accurately representing the state without approximation.

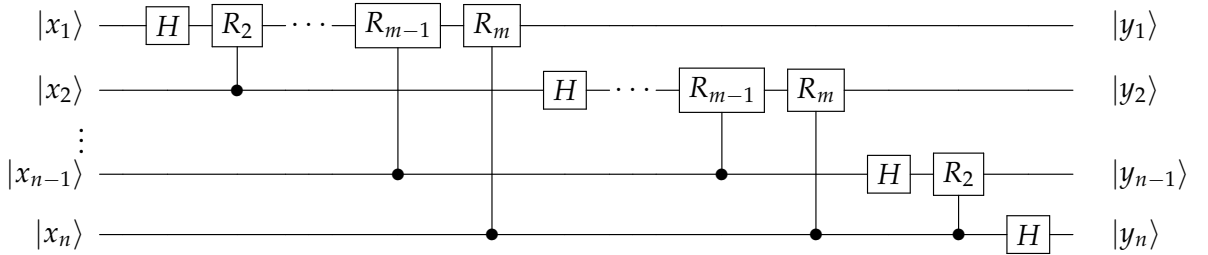


Figure 4: Temp

The rotation  $R_k$  in figure 4 is defined as the controlled version of

$$R_k = \begin{pmatrix} 1 & 0 \\ 0 & e^{\frac{2\pi i}{2^k}} \end{pmatrix}. \tag{26}$$

To verify that this circuit is the QFT, consider the state  $|x_1 \cdots x_n\rangle$  as input. Applying the Hadamard gate on the first qubit produces the state

$$H |x_1 \cdots x_n\rangle = \frac{1}{\sqrt{N}}(|0\rangle + e^{2\pi i 0.x_1} |1\rangle) |x_1 \cdots x_n\rangle. \quad (27)$$

The next operation is the rotation  $R_2$ , controlled by the second qubit, resulting in state

$$\frac{1}{\sqrt{N}}(|0\rangle + e^{2\pi i 0.x_1 x_2} |1\rangle) |x_1 \cdots x_n\rangle. \quad (28)$$

Applying the successive rotations up to  $R_n$  appends an extra bit to the phase of the first  $|1\rangle$ , ultimately becoming

$$\frac{1}{\sqrt{N}}(|0\rangle + e^{2\pi i 0.x_1 x_2 \cdots x_n} |1\rangle) |x_1 \cdots x_n\rangle. \quad (29)$$

A similar process is applied to the second qubit, and at the end of the rotations the state is

$$\frac{1}{\sqrt{N}}(|0\rangle + e^{2\pi i 0.x_1 x_2 \cdots x_n} |1\rangle)(|0\rangle + e^{2\pi i 0.x_2 \cdots x_n} |1\rangle) |x_1 \cdots x_n\rangle, \quad (30)$$

and the successive application of this process to the remaining qubits results in state

$$\frac{1}{\sqrt{N}}(|0\rangle + e^{2\pi i 0.x_1 x_2 \cdots x_n} |1\rangle)(|0\rangle + e^{2\pi i 0.x_2 \cdots x_n} |1\rangle) \cdots (|0\rangle + e^{2\pi i 0.x_n} |1\rangle) |x_1 \cdots x_n\rangle, \quad (31)$$

confirming that this is indeed the Fourier transform derived in equation 25 minus the order of the qubits, which is reversed. It also shows that the QFT is unitary, since all operations in the circuit are unitary.

Counting the number of gates on the circuit, one can conclude that the first qubit will have 1 Hadamard gate followed by  $n - 1$  controlled rotations. The second qubit is another Hadamard followed by  $n - 2$  controlled rotations. After  $n$  qubits, the total number of gates will be  $\frac{n(n+1)}{2}$ . This means the circuit provides a  $O(n^2)$  algorithm, compared to the fastest classical algorithm, the *Fast Fourier Transform* which requires  $O(n2^n)$  operations. This is an exponential gain, which can be improved upon at the cost of accuracy, but it's not a replacement for calculating classical Fourier transforms for the aforementioned reasons.

---

## QUANTUM WALKS

---

### 3.1 CLASSICAL RANDOM WALK

The term *random walk*, firstly introduced by [Pearson \(1905\)](#), is classically defined as a stochastic process that models the path a walker would take through a mathematical space, where each step made by the walker is random. This can be used to model systems such as a molecule displaying Brownian motion in a fluid, or even fluctuating stock prices as can be seen in [Sottinen \(2001\)](#).

The simplest instance of this walk is on a discretely numbered line, whose mathematical space is composed of integer numbers. Here, the walker can only advance with equal probability in one of two directions, depending on the outcome of a random event such as tossing a coin. This was coded in Python, and the result of iterating the walk several times is a binomial distribution centered around the starting position.

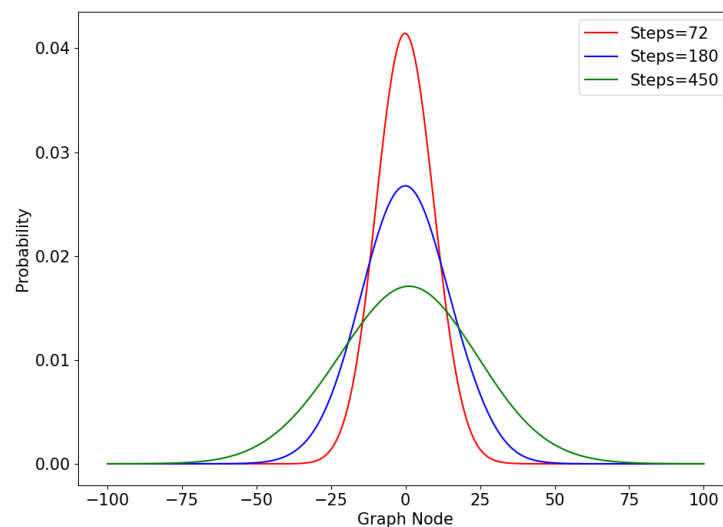


Figure 5: Classical Walk Temp.



The number of steps (iterations) directly affects how far the walker can reach, as can be seen in figure 5. As the number of steps increases, the height of each curve at the starting position decreases and the width of the curves increases. This relationship can be captured by the *position standard deviation*, and Portugal (2018) shows that the standard deviation is

$$\sigma(t) = \sqrt{t}. \quad (32)$$

In other words, equation 32 represents the rate at which a walker moves away from the origin.

Note that this algorithm can be abstracted to graphs of higher dimensions. For example, in a two dimensional lattice, a walker would be transversing a plane with integer coordinates, choosing one of four directions in every intersection. Notably, Pólya (1921) proved that a walker in a two dimensional lattice will almost surely return to the origin at some point. However, the probability of returning to the origin decreases as the number of dimensions increases, as shown by Montroll (1956) and Finch (2003).

It is worth noting that a random walk, over a graph whose nodes are weighed and directed, is analagous to a *discrete-time Markov chain*<sup>1</sup>.

The following sections will be used to describe various models of a quantum counterpart of the classical random walk.

### 3.2 COINED QUANTUM WALK

In the quantum case, the walker is a quantum system whose position on a discretely numbered line, is described by a vector  $|x\rangle$  in Hilbert Space. The next position of the system will depend, in part, of a unitary operator, which can be viewed as a quantum coin. The analogy is, if the coin is tossed and rolls "heads", for example, the system transitions to position  $|x + 1\rangle$ , otherwise it advances to  $|x - 1\rangle$ . From a physical perspective, this coin can be the spin of an electron or the chirality of a particle, for example, and the outcome of measuring these properties decides whether the walker moves left or right. The coin is a unitary operator defined as

$$\begin{cases} C |0\rangle |x\rangle = a |0\rangle |x\rangle + b |1\rangle |x\rangle \\ C |1\rangle |x\rangle = c |0\rangle |x\rangle + d |1\rangle |x\rangle, \end{cases} \quad (33)$$

<sup>1</sup> A Markov chain can be described as a sequence of stochastic events where the the probability of each event depends only on the state of the previous event.

where  $a, b, c$  and  $d$  are the amplitudes associated with each outcome of the coin toss. One of the most commonly used coins is the unbiased coin, also known as Hadamard operator

$$H = \begin{pmatrix} a & c \\ b & d \end{pmatrix} = \frac{1}{\sqrt{2}} \begin{pmatrix} 1 & 1 \\ 1 & -1 \end{pmatrix}, \quad (34)$$

which will be the one used in this example.

The Hilbert space of the system is  $\mathcal{H} = \mathcal{H}_C \otimes \mathcal{H}_P$ , where  $\mathcal{H}_C$  is the two-dimensional Hilbert space associated with the coin and  $\mathcal{H}_P$  is the Hilbert space of the walker.

The transition from  $|x\rangle$  to either  $|x+1\rangle$  or  $|x-1\rangle$  must be described by a unitary operator, the *shift operator*

$$\begin{cases} \mathcal{S} |0\rangle |x\rangle = |0\rangle |x+1\rangle \\ \mathcal{S} |1\rangle |x\rangle = |1\rangle |x-1\rangle, \end{cases} \quad (35)$$

that can also be described by

$$S = |0\rangle \langle 0| \otimes \sum_{x=-\infty}^{x=\infty} |x+1\rangle \langle x| + |1\rangle \langle 1| \otimes \sum_{x=-\infty}^{x=\infty} |x-1\rangle \langle x|. \quad (36)$$

It follows that the operator that describes the dynamics of the quantum walk will be given by

$$U = S(C \otimes I) = S(H \otimes I). \quad (37)$$

Consider a quantum system located at  $|x=0\rangle$  with coin state  $|0\rangle$ , for  $t=0$ . It's state will be described by

$$|\Psi(0)\rangle = |0\rangle |x=0\rangle. \quad (38)$$

After  $t$  steps

$$|\Psi(t)\rangle = U^t |\Psi(0)\rangle, \quad (39)$$

more explicitly

$$|\Psi(0)\rangle \xrightarrow{U} |\Psi(1)\rangle \xrightarrow{U} |\Psi(2)\rangle \xrightarrow{U} \dots \xrightarrow{U} |\Psi(t)\rangle. \quad (40)$$

In other words, the coined quantum walk algorithm consists on applying the coin operator followed by the shift operator a certain number of times. Iterating this twice, evolves the system to the following respective states

$$|\Psi(1)\rangle = \frac{|0\rangle |x=-1\rangle + |1\rangle |x=1\rangle}{\sqrt{2}} \quad (41)$$

$$|\Psi(2)\rangle = \frac{|0\rangle |x=-2\rangle + |1\rangle |x=0\rangle + |0\rangle |x=0\rangle - |1\rangle |x=2\rangle}{2} \quad (42)$$

$$(43)$$

If one were to measure the system after the first application of  $\mathcal{U}$ , it would be expected to see the walker at  $x = 1$  with probability  $P(x) = \frac{1}{2}$ , and at  $x = -1$  with  $P(x) = \frac{1}{2}$  aswell. Measure the system  $t$  times, after each application of  $\mathcal{U}$ , and the result is a binomial probability distribution similar to the one in 5. The conclusion is that repetitive measurement of a coined quantum walk system reduces to the classical case, which means that any desired quantum behaviour is lost.

It is possible, however, to make use of the quantum correlations between different positions to generate constructive or destructive interference, by applying the Hadamard and shift operators successively without intermediary measurements. The consequences of interference between states become very apparent after only 3 iterations

$$|\Psi(3)\rangle = \frac{|1\rangle |x = -3\rangle - |0\rangle |x = -1\rangle + 2(|0\rangle + |1\rangle) |x = 1\rangle + |0\rangle |x = 3\rangle}{2\sqrt{2}}. \quad (44)$$

Even though an unbiased coin was used, this state is not symmetric around the origin and the probability distributions will not be centered in the origin. Moreover, [Portugal \(2018\)](#) shows that the standard deviation will be

$$\sigma(t) \approx 0.54t. \quad (45)$$

This means that the standard deviation for the coined quantum walk grows linearly in time, unlike the classical case which grows with  $\sqrt{t}$ , as was seen in equation 32. The implication is that the quantum walk displays *ballistic* behaviour, as is reviewed in [Venegas-Andraca \(2012\)](#). This behaviour is usually defined in the context of a moving free particle with unit velocity in a single direction, which is expected to be found at  $x = t$  after  $t$  steps. The velocity of a walker in a Hadamard quantum walk is approximately half of the free particle example, which is still a quadratic improvement over the classical random walk.

This quadratic gain implies exponentially faster hitting times in certain graphs, as shown by [Childs et al. \(2002\)](#), meaning improvements to problems that require transversing graphs. [Ambainis \(2007\)](#) also shows advantages of the coined quantum walk model in element distinctness problems, and [Childs and Goldstone \(2004\)](#) show advantages in spatial search problems, which will be studied in a later chapter.

In order to study this distribution, a simulation of the coined quantum walk was coded in *Python*. Figure 6 is the result of using the Hadamard coin and the initial condition in equation 38, for varying numbers of steps. Analyzing the plot, it is noticeable that the distributions are asymmetric. The probability of finding the walker on the right-hand side is much larger than on the left, with a peak around  $x \approx \frac{t}{\sqrt{2}}$ . Regardless of number of steps, this peak is always present (albeit in varying positions), which is to say that the walker can always be found moving in a uniform fashion away from the origin, consistent with ballistic behaviour.

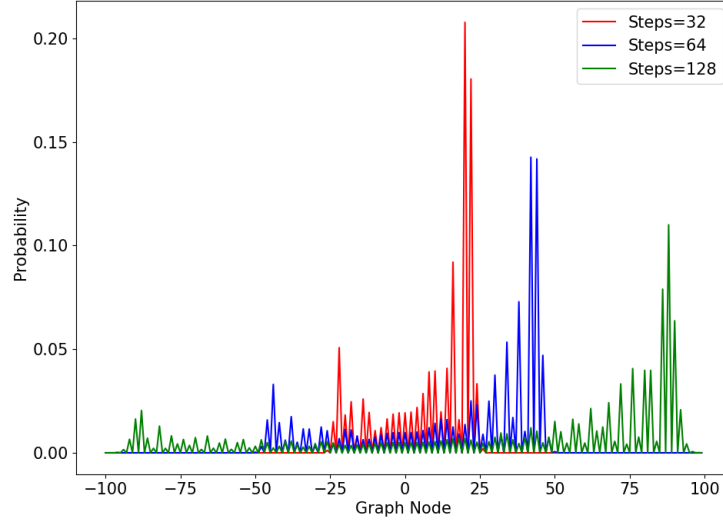


Figure 6: Probability distribution for the coined quantum walk on a line, after 100 steps, with initial condition  $|\Psi(0)\rangle = |0\rangle |x = 0\rangle$  and the Hadamard coin.

Another interesting case study is to find if this behaviour is preserved for a symmetric distribution around the origin. For this purpose, one must first understand where the asymmetry comes from. The Hadamard operator flips the sign of state  $|1\rangle$ , hence more

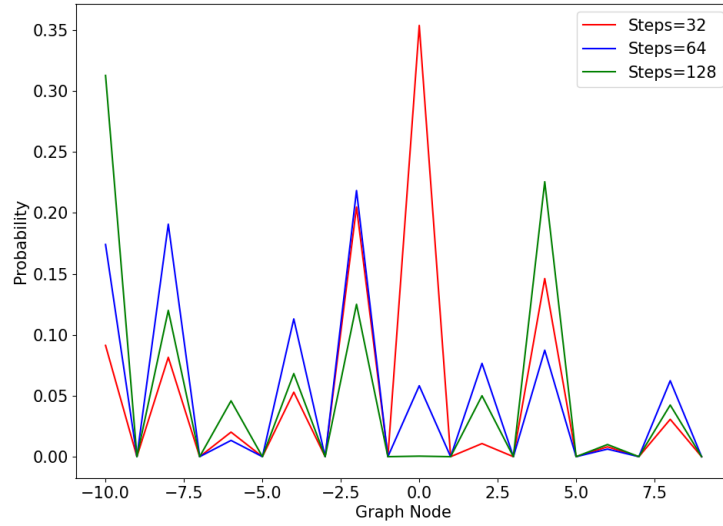


Figure 7: Probability distribution for the coined quantum walk on a line, after 100 steps, with initial condition  $|\Psi(0)\rangle = -|1\rangle |x = 0\rangle$  and the Hadamard coin.

terms are cancelled when the coin state is  $|1\rangle$ . Since  $|0\rangle$  was defined to induce movement

to the right, the result is as shown in 6. Following this logic, it would be expected that an initial condition

$$|\Psi(0)\rangle = |1\rangle |x=0\rangle, \quad (46)$$

would result in more cancellations when the coin state is  $|0\rangle$ , thus the walker would be more likely found in the left-hand side of the graph. This is indeed what happens, as figure 7 is a mirror image of figure 6. The walker still moves away from the origin with ballistic behaviour, but in opposite direction. The peaks behave in a similar fashion, being instead found at  $x \approx -\frac{t}{\sqrt{2}}$ .

In order to obtain a symmetrical distribution, one must superpose the state in equation 38 with the state in equation 46. However, in order to not cancel terms before the calculation of the probability distribution, one must multiply state  $|1\rangle$  with the imaginary unit,  $i$

$$|\Psi(0)\rangle = \frac{|0\rangle + i|1\rangle}{\sqrt{2}} |x=0\rangle. \quad (47)$$

This works because the entries of the Hadamard operator are real numbers. Terms with the imaginary unit will not cancel out with terms without it, thus the walk can proceed to both left and right, as it is shown in figure 8.

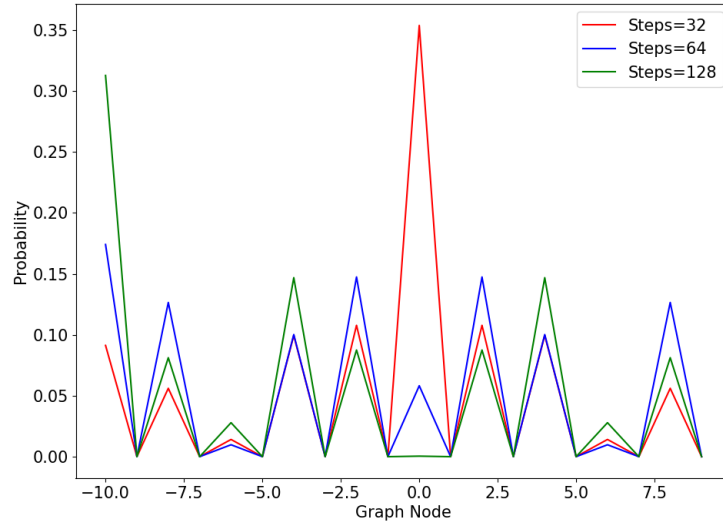


Figure 8: Probability distribution for the coined quantum walk on a line, after 100 steps, with initial condition  $|\Psi(0)\rangle = \frac{|0\rangle - i|1\rangle}{\sqrt{2}} |x=0\rangle$  and the Hadamard coin.

The probability distribution is now symmetric and it is spread over the range  $[-\frac{t}{\sqrt{2}}, \frac{t}{\sqrt{2}}]$  with peaks around  $|x| \approx \pm \frac{t}{\sqrt{2}}$ . This means that if the position of the walker was measured

at the end, it would be equally probable to find him either in the left side or the right side of the graph, which is not possible in a classical ballistic motion.

All of the previous examples are in sharp contrast with the classical random walk distribution in figure 5. There, maximum probability is reached at  $x = 0$  since there are approximately equal steps in both directions. Furthermore, the further the vertex is away from the origin, the less likely the walker is to be found there. However, in the quantum case, the walker is more likely to be found away from the origin as the number of steps increases. More specifically, the walk spreads quadratically faster than the classical counterpart.

This is but one model of a quantum random walk. As it will be seen in further sections, there are other approaches to creating both discrete and continuous quantum walk models that do not use a coin.

### 3.3 CONTINUOUS-TIME QUANTUM WALK

The continuous-time random walk model on a graph is a Markov process where transitions have a fixed probability per unit time  $\gamma$  of moving to adjacent vertices, firstly introduced by [Montroll and Weiss \(1997\)](#). Consider a graph  $G$  with  $N$  vertices and no self-loops, this walk can be defined by the linear differential equation that describes the probability of jumping to a connected vertex in any given time

$$\frac{dp_i(t)}{dt} = \gamma \sum_j L_{ij} p_j(t), \quad (48)$$

where  $L$  is the Laplacian defined as  $L = A - D$ .  $A$  is the adjacency matrix that represents each vertex connection, given by

$$A_{ij} = \begin{cases} 1, & \text{if } (i, j) \in G \\ 0, & \text{otherwise,} \end{cases} \quad (49)$$

and  $D$  is the diagonal matrix  $D_{jj} = \deg(j)$  corresponding to the degree<sup>2</sup> of a vertex  $j$ .

In the quantum case, the nodes are quantum states that form the basis for the Hilbert space. The continuous-time quantum walk model will also be described by a differential equation, the Schrödinger equation

$$i\hbar \frac{d|\Psi(t)\rangle}{dt} = \hat{H} |\Psi(t)\rangle, \quad (50)$$

---

<sup>2</sup> The degree of a vertex refers to the number of edges that it is connected to.

where  $\hat{H} = -\gamma L$  is the Hamiltonian of the system. More explicitly,

$$\hat{H}_{ij} = \begin{cases} \deg(j)\gamma, & \text{if } i = j; \\ -\gamma, & \text{if } i \neq j \text{ and adjacent;} \\ 0, & \text{if } i \neq j \text{ and not adjacent.} \end{cases} \quad (51)$$

A general state of a system  $|\Psi(t)\rangle$  can be written as a function of its complex amplitudes

$$q_i = \langle i | \Psi(t) \rangle, \quad (52)$$

which means 50 can be rewritten as

$$i\hbar \frac{dq_i(t)}{dt} = \sum_j \hat{H}_{ij} q_j(t). \quad (53)$$

This highlights the similarities between the Schrödinger equation and 48. One of the main differences is the complex phase  $i$ , which will result in a very different behaviour. Setting  $\hbar = 1$  and solving the differential equation results in the evolution operator of this walk

$$U(t) = e^{-iHt} = e^{i(-\gamma L)t} = e^{-i\gamma(A+D)t} \quad (54)$$

In the regular graph case, where  $D$  is simply the degree of the whole graph multiplied by the identity matrix,  $A$  and  $D$  will commute, meaning that the evolution operator can be written in terms of the adjacency matrix

$$U(t) = e^{-i\gamma At + i\gamma Dt} = e^{-i\gamma At} e^{i\gamma Dt} = \phi(t) e^{-i\gamma At} \quad (55)$$

since the degree matrix becomes a global phase. Applying this operator to an initial condition  $\Psi(0)$ , will give the state of the system at a time  $t$

$$|\Psi(t)\rangle = U(t) |\Psi(0)\rangle. \quad (56)$$

Considering a uni-dimensional quantum system, each vertex will have at most 2 other neighboring vertices, reducing equation 51 to

$$\hat{H}_{ij} = \begin{cases} 2\gamma, & \text{if } i = j; \\ -\gamma, & \text{if } i \neq j \text{ and adjacent;} \\ 0, & \text{if } i \neq j \text{ and not adjacent.} \end{cases} \quad (57)$$

For a more detailed visualization, this quantum walk model was coded in python and figure 9 was obtained setting the transition rate to  $\gamma = \frac{1}{2\sqrt{2}}$  the initial condition to  $|\Psi(0)\rangle = |0\rangle$

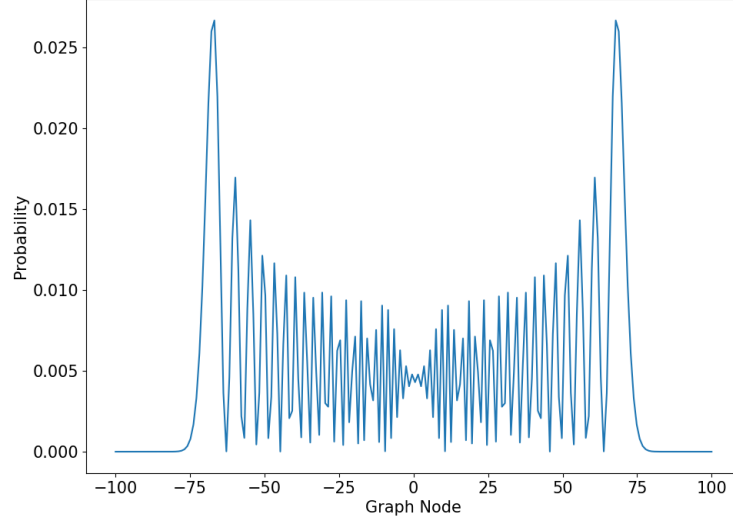


Figure 9: Probability distribution for the continuous-time quantum walk on a line, at  $t = 100$ , with initial condition  $|\Psi(0)\rangle = |0\rangle$  and  $\gamma = \frac{1}{2\sqrt{2}}$ .

A brief look at figure 9 reveals several similarities to the coined quantum walk model of figure ???. Both have two peaks away from the origin and low probability near the origin. However, in the previous quantum walk, these characteristics were altered as a function of the chosen coin and initial condition, whereas in this case different values of  $\gamma$  will influence the probability distribution. For example, a lower value of  $\gamma$  will limit the spread of the probability distribution, as is shown in figure 11.

Moreover, the effects of altering the initial condition will also differ in the continuous-time example. For example, setting the initial condition to the balanced superposition of states  $|0\rangle$  and  $|1\rangle$  has no effect on the overall pattern of the probability distribution as can be seen in figure 13. Both peaks still are still present and at the same distance from the origin, with intermediate amplitudes being attenuated relative to figure 9. This behaviour is in contrast with the discrete-time case, where a change in the initial condition would dictate the number of peaks and where they would appear.



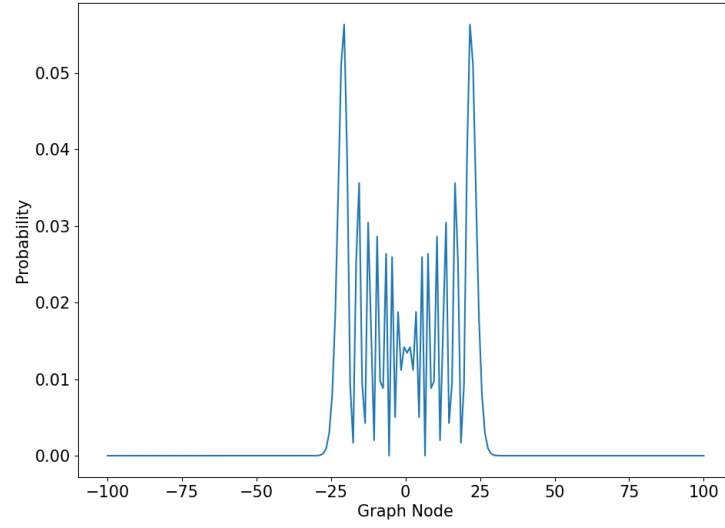


Figure 10: Probability distribution for the continuous-time quantum walk on a line, after 100 steps, with initial condition  $|\Psi(0)\rangle = |0\rangle$  and  $\gamma = \frac{1}{6\sqrt{2}}$ .

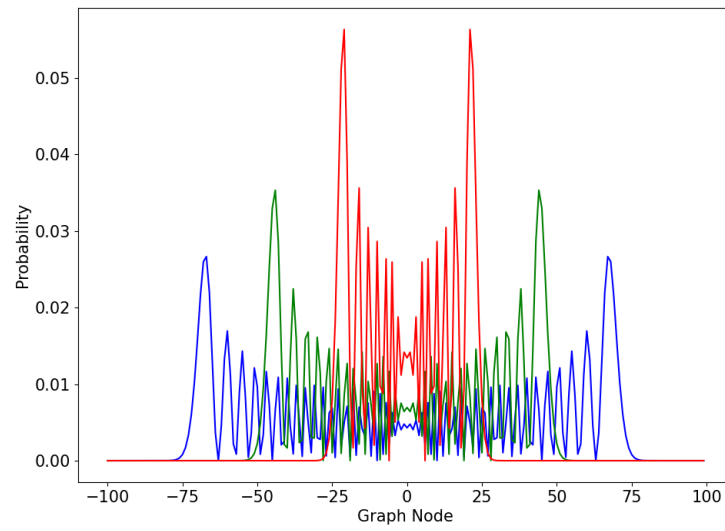


Figure 11: Temporary

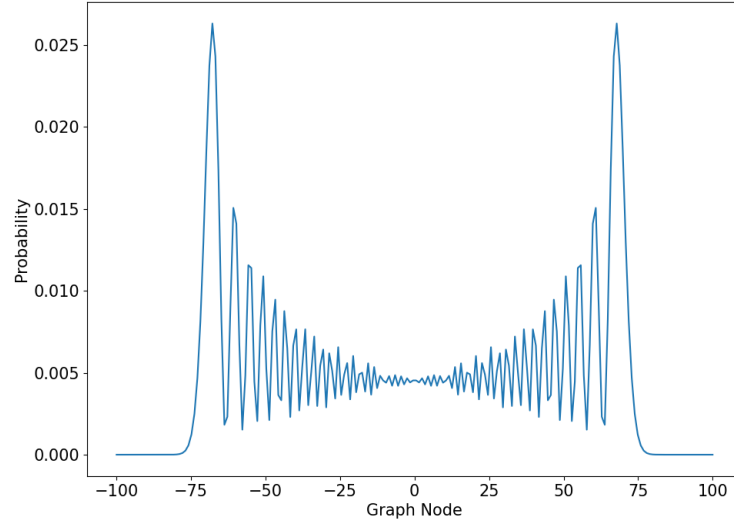


Figure 12: Probability distribution for the continuous-time quantum walk on a line, after 100 steps, with initial condition  $|\Psi(0)\rangle = \frac{|0\rangle + |1\rangle}{\sqrt{2}}$  and  $\gamma = \frac{1}{2\sqrt{2}}$ .

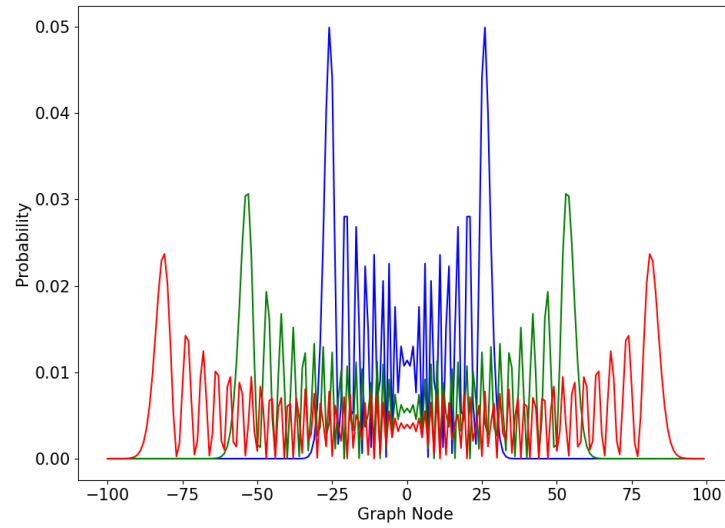


Figure 13: Temporary

## 3.4 STAGGERED QUANTUM WALK

Similarly to the continuous-time quantum walk, the staggered case aims to spread a transition probability to neighboring vertices but with discrete time steps. The notion of adjacency now comes from cliques<sup>3</sup>, and the initial stage of this walk consists in partitioning the graph in several different cliques. This is called tessellation, and it is defined as the division of the set of vertices into disjoint cliques. An element of a tessellation  $\mathcal{T}$  is called a polygon, and it's only valid if all of its vertices belong to the clique in  $\mathcal{T}$ . The set of polygons of each tessellation must cover all vertices of the graph, and the set of tessellations  $(\mathcal{T}_1, \mathcal{T}_2, \dots, \mathcal{T}_k)$  must cover all edges.

These definitions allow the construction of operators  $H_1, H_2, \dots, H_k$  that will be used to propagate the probability amplitude locally, in each polygon. The state associated to each polygon is

$$|u_j^k\rangle = \frac{1}{\sqrt{|\alpha_j^k|}} \sum_{l \in \alpha_j^k} |l\rangle \quad (58)$$

where  $\alpha_j^k$  is the  $j$ -th polygon in the  $k$ -th tessellation.

The unitary and Hermitian operator  $H_k$ , associated to each tessellation is defined in [Portugal et al. \(2017\)](#) as

$$H_k = 2 \sum_{j=1}^p |u_j^k\rangle \langle u_j^k| - I \quad (59)$$

Solving the time-independent Schrodinger equation for this Hamiltonian gives the evolution operator

$$U = e^{i\theta_k H_k} \dots e^{i\theta_2 H_2} e^{i\theta_1 H_1} \quad (60)$$

where

$$e^{i\theta_k H_k} = \cos(\theta_k)I + i \sin(\theta_k)H_k \quad (61)$$

since  $H_k^2 = I$ .

The simplest use case of this quantum walk model is the one-dimensional lattice, where the minimum tessellations are

$$\mathcal{T}_\alpha = \{\{2x, 2x+1\} : x \in \mathbb{Z}\} \quad (62)$$

$$\mathcal{T}_\beta = \{\{2x+1, 2x+2\} : x \in \mathbb{Z}\} \quad (63)$$

<sup>3</sup> A clique is defined as the subset of vertices of an undirected graph such that every two distinct vertices in each clique are adjacent.

Each element of the tessellation has a corresponding state, and the uniform superposition of these states is

$$|\alpha_x\rangle = \frac{|2x\rangle + |2x+1\rangle}{\sqrt{2}} \quad (64)$$

$$|\beta_x\rangle = \frac{|2x+1\rangle + |2x+2\rangle}{\sqrt{2}} \quad (65)$$

One can now define Hamiltonians  $H_\alpha$  and  $H_\beta$  as

$$H_\alpha = 2 \sum_{x=-\infty}^{+\infty} |\alpha_x\rangle \langle \alpha_x| - I \quad (66)$$

$$H_\beta = 2 \sum_{x=-\infty}^{+\infty} |\beta_x\rangle \langle \beta_x| - I \quad (67)$$

The Hamiltonian evolution operator reduces to

$$U = e^{i\theta H_\beta} e^{i\theta H_\alpha} \quad (68)$$

and applying it to an initial condition  $|\Psi(0)\rangle$  results in the time evolution operator

$$U |\Psi(t)\rangle = U^t |\Psi(0)\rangle \quad (69)$$

Having defined the time evolution operator, the walk is ready to be coded with a certain initial condition and  $\theta$  value, to better understand how the probability distribution spreads through time.

For the first case study, the initial condition will be a uniform superposition of states  $|0\rangle$  and  $|1\rangle$  and the  $\theta$  value will be varied in order to understand how this parameter impacts the walk

The overall structure of the probability distribution remains the same, the difference is that the walker is more likely to be found further away from the origin as the angle increases.

Another interesting case study is to see how the initial condition affects the dynamics of the system

Similarly to the coined case, each initial condition results in asymmetric probability distributions,  $|\Psi(0)\rangle = |0\rangle$  leads to a peak in the left-hand side while condition  $|\Psi(0)\rangle = |1\rangle$  results in a peak in the right-hand side. As was shown in 14, the uniform superposition of both these conditions results in a symmetric probability distribution.

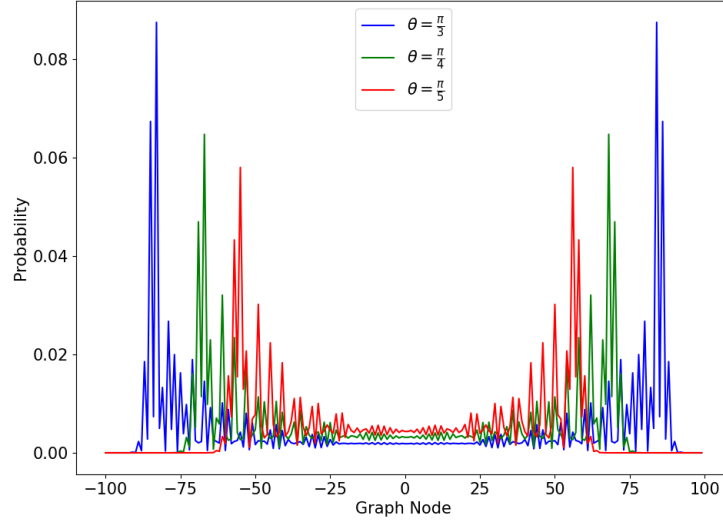


Figure 14: Probability distribution for the staggered quantum walk on a line after 50 steps, with initial condition  $|\Psi(0)\rangle = \frac{|0\rangle + |1\rangle}{\sqrt{2}}$ , for multiple angles.

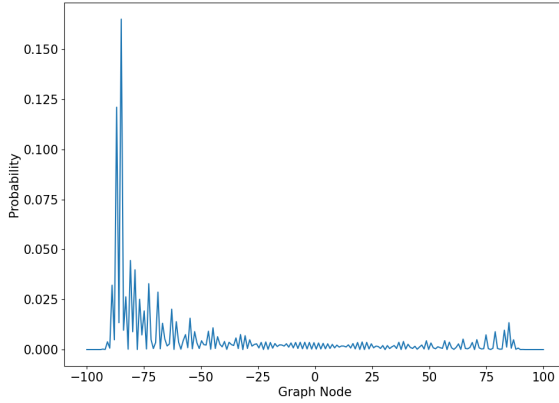


Figure 15:  $|\Psi(0)\rangle = |0\rangle$

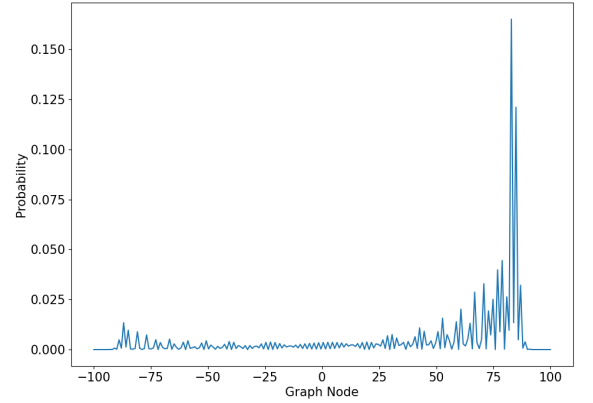


Figure 16:  $|\Psi(0)\rangle = |1\rangle$

### 3.5 SEARCH PROBLEMS WITH QUANTUM WALKS

In classical computation, a *spatial search problem* focuses on finding marked points in a finite region of space. Defining this region with graphs is fairly straightforward, the vertices of the graph are the search space, and the edges define what transitions are possible through the search space. As was previously mentioned in ??, exhaustively searching through an unstructured space, by means of a classical random walk for example, would mean that in the worst case, one would have to take as many steps to find the marked points as there

are vertices in the graph. Quantum computing provides an alternative to this complexity through Grover's algorithm, and applying some of his ideas to the coined quantum walk not only allows a quantum counterpart to the random walk search, but also further insight into the algorithm itself.

### 3.5.1 Coined

Following [Portugal \(2018\)](#)'s definition, a good first step is to borrow the diffusion from Grover's algorithm and invert the sign of the state corresponding to the marked vertex while leaving unmarked vertices unchanged. This is done through the following operator

$$\mathcal{O} = I - 2 \sum_{x \in M} |x\rangle \langle x| \quad (70)$$

where  $M$  is the set of marked vertices and  $\mathcal{O}$  is an analogue to Grover's oracle. For one marked vertex, this oracle can be written as

$$\mathcal{O} = I - 2 |0\rangle \langle 0| \quad (71)$$

Notice that there is no loss of generality by choosing the marked vertex as 0, since the labelling of the vertices is arbitrary.

The next step is to combine the evolution operator from the coined quantum walk model with the oracle

$$U' = U\mathcal{O} \quad (72)$$

Similarly to the simple coined case, the walker starts at  $|\Psi(0)\rangle$  and evolves following the rules of an unitary operator  $U$  followed by the sign inversion of marked vertices. The walker's state after an arbitrary number of steps will be

$$\Psi(t) = (U')^t |\Psi(0)\rangle. \quad (73)$$

For a better understanding of the search problem in the coined quantum walk model, consider a graph where all the vertices are connected and each vertex has a loop that allows transitions to itself, as shown in figure ?? . The next step is to label the arcs using notation  $\{(v, v'), v \geq 0 \wedge v' \leq N - 1\}$  where  $N$  is the total number of vertices and  $(v, v')$  are the position and coin value, respectively, in the coined model. The shift operator, now called *flip-flop* shift operator, is

$$S |v1\rangle |v2\rangle = |v2\rangle |v1\rangle. \quad (74)$$

The coin operator is defined as

$$C = I_N \otimes G \quad (75)$$

where

$$G = 2 |D\rangle \langle D| - I \quad (76)$$

is the Grover coin with  $|D\rangle$  being the diagonal state of the coin space. Given both of these operators, the evolution is defined for the unmarked case similarly to ??

$$U = S(I \otimes G). \quad (77)$$

Marking an element in a complete graph is done through the following oracle

$$\mathcal{O}' = \mathcal{O} \otimes I = (I_N - 2 |0\rangle \langle 0|) \otimes I_N = I_{N^2} - 2 \sum_v |0\rangle |v\rangle \langle 0| \langle v|, \quad (78)$$

that can be seen, in the arc notation, as an operator that marks all arcs leaving 0.

Recalling 72, the modified evolution operator can be written as

$$U' = S(I \otimes G) \mathcal{O}' = S(I \otimes G) \mathcal{O} \otimes I = S(\mathcal{O} \otimes G), \quad (79)$$

and the state of the system will evolve according to equation 73.

As was shown in Portugal (2018), maximum probability of the marked vertex is achieved after  $\frac{\pi}{2} \sqrt{N}$  steps. Figure 17 is the result of coding and plotting the evolution of this probability distribution, for graphs of varying sizes. It shows that the probability is close to one at *approximately* the predicted ideal steps, because of the discrete nature of the walk. The probability distributions have a stair-like shape, because transitions in this model only occur on even numbered time steps, because of how the unmodified evolution operator was constructed.

### 3.5.2 Staggered

The process for defining the search problem in this model is similar to the coined quantum walk case. The oracle still inverts the sign of a certain state and amplifies it, and the system's state will still be described by equation 73. However, instead of using a coin, the staggered model takes advantage of the notions of cliques and tessellations, as was shown in chapter ??, which means the unmodified evolution operator has to be defined for an undirected complete graph.

As was shown in figure ??, the vertices in a complete graph are all neighbors. This is a special case because this is the only connected graph where the tessellation cover can be done by one tessellation, since the graph is its own clique. The minimum tessellations required to cover this structures are defined by the one clique that encompasses all  $N$  nodes of the graph

$$\mathcal{T}_\alpha = \{\{0, 1, 2, \dots, N-1\}\}. \quad (80)$$

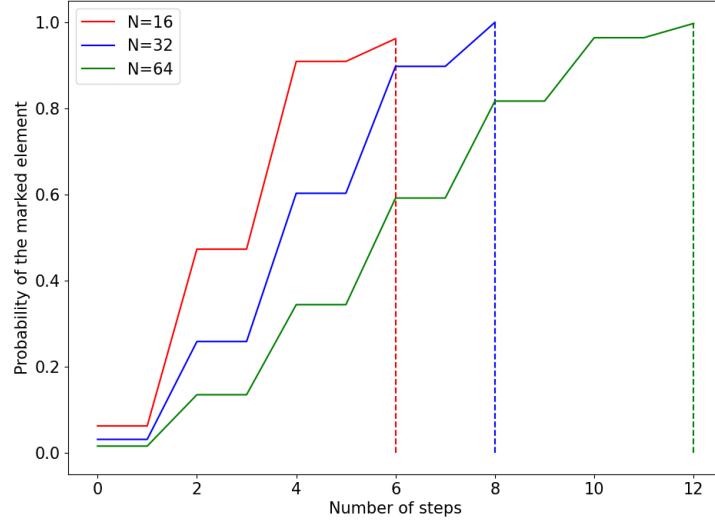


Figure 17: Discrete-time coined quantum walk search for a complete graph with 16, 32 and 64 nodes.

The associated polygon can then be described as the balanced superposition of all the nodes in the graph

$$|\alpha\rangle = \frac{1}{\sqrt{N}} \sum_{v=0}^{N-1} |v\rangle. \quad (81)$$

The Hamiltonian, as defined in 59, is

$$H_\alpha = 2 \sum_0^1 |\alpha\rangle \langle \alpha| - I = 2 |\alpha_0\rangle \langle \alpha_0| - I \quad (82)$$

The unmodified evolution operator from equation 60

$$U = e^{i\theta_k H_k} \dots e^{i\theta_2 H_2} e^{i\theta_1 H_1} \quad (83)$$

reduces to the single Hamiltonian case

$$U = e^{i\theta H_\alpha}. \quad (84)$$

The choice of the  $\theta$  value is an important one, since maximum probability is achieved at  $\theta = \frac{\pi}{2}$ , as shown in figure 18. Since  $H_\alpha^2 = I$ , equation 84 can be rewritten as

$$U = e^{-i\frac{\pi}{2} H_\alpha} = \cos \frac{\pi}{2} I + i \sin \frac{\pi}{2} H_\alpha = i H_\alpha = i(2 |\alpha_0\rangle \langle \alpha_0| - I). \quad (85)$$



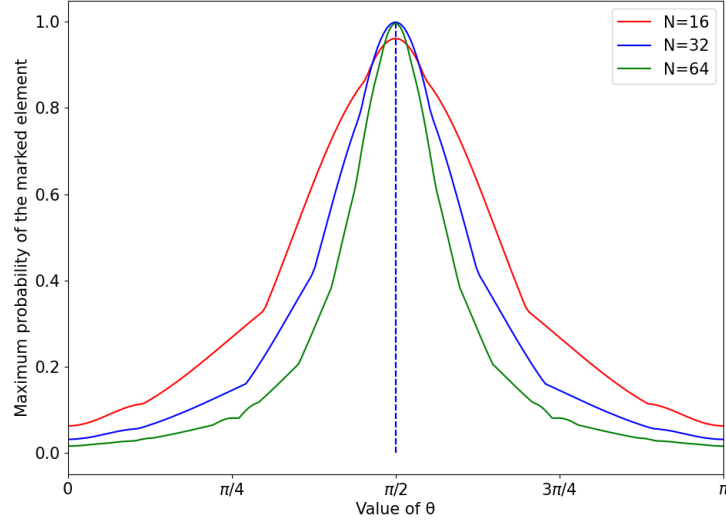


Figure 18: Maximum probability of the marked element as a function of the  $\theta$  value plotted from 0 to  $\pi$  for number of nodes  $N = 64, 128$  and  $256$ .

Having defined the the evolution operator associated with the complete graph, the next step is to use the oracle

$$\mathcal{O} = I_N - 2 |0\rangle \langle 0|, \quad (86)$$

to create the modified evolution operator associated with the search

$$U' = U\mathcal{O}. \quad (87)$$

The walk achieves the same result as Grover's algorithm after  $\frac{\pi}{4}\sqrt{N}$  steps, as shown in figure 19. This plot also shows that the probabilities converge to 1 as  $N$  increases, this is because time is discretized and deviations to the ideal steps will matter less for bigger values of  $N$ .

### 3.5.3 Continuous

As was previously seen, the continuous-time quantum walk model is defined by an evolution operator obtained by solving Schrödinger's equation

$$U(t) = e^{-iHt}. \quad (88)$$

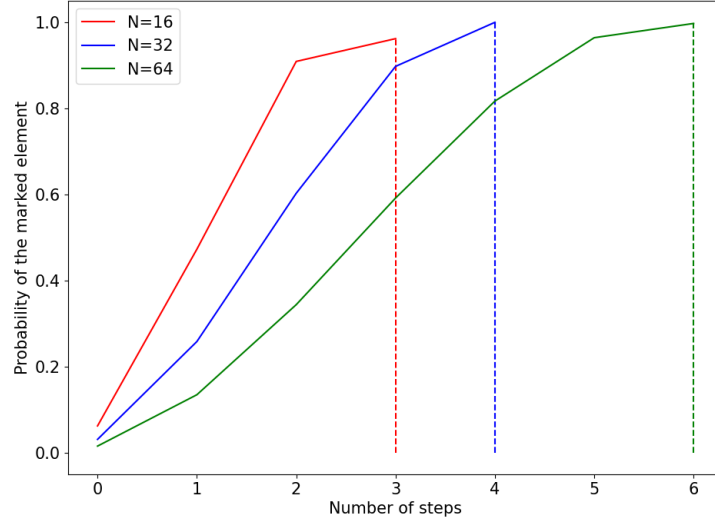


Figure 19: Staggered quantum walk search for a complete graph with 16, 32 and 64 nodes.

The search problem requires introducing an oracle to the Hamiltonian, that will mark an arbitrary vertex  $m$

$$H' = -\gamma L - |m\rangle \langle m|. \quad (89)$$

Since the complete graph is a regular graph, the operator can be rewritten in terms of the adjacency matrix plus the marked element. Considering  $|0\rangle$  is marked,

$$U'(t) = e^{iH't} = e^{i(-\gamma L - |0\rangle \langle 0|)t} = e^{i(-\gamma A + \gamma D - |0\rangle \langle 0|)t} = e^{-i\gamma(A + |0\rangle \langle 0|)t + i\gamma Dt}. \quad (90)$$

The degree matrix is again  $D = dI$ , which means it will commute with  $A + |0\rangle \langle 0|$  and become a global phase

$$U'(t) = e^{-i\gamma(A + |0\rangle \langle 0|)t} e^{i\gamma Dt} = \phi(t) e^{-i\gamma(A + |0\rangle \langle 0|)t}. \quad (91)$$

As was show by [Zalka \(1999\)](#), the value of  $\gamma$  is crucial for the success of the search. As  $\gamma$  increases, the contribution of the marked element in the Hamiltonian decreases, and as  $\gamma$  approaches 0 the contribution of the adjacency matrix decreases. To find the optimum value, the Hamiltonian can be rewritten by adding multiples of the identity matrix to the adjacency matrix

$$H' = -\gamma(A + NI) - |0\rangle \langle 0| = -\gamma N |s\rangle \langle s| - |0\rangle \langle 0| \quad (92)$$

where  $|s\rangle = \frac{1}{\sqrt{N}} \sum_i |i\rangle$ . Now it is obvious that, for  $\gamma = \frac{1}{N}$ , the Hamiltonian is  $H = -|s\rangle\langle s| - |0\rangle\langle 0|$ . Its eigenstates are proportional to  $|s\rangle \pm |w\rangle$  and eigenvalues are  $-1 - \frac{1}{\sqrt{N}}$  and  $-1 + \frac{1}{\sqrt{N}}$ , respectively. This means that the evolution rotates from the state of balanced superposition to the marked vertex state in time  $\frac{\pi}{\Delta E} = \frac{\pi}{2}\sqrt{N}$  which is, as was shown by [Zalka \(1999\)](#), optimal and equivalent to Grover's algorithm. Plotting  $\Delta E$  as a function of  $\gamma N$ , as can be seen in figure 20, has a minimum at  $\gamma N = 1$ . The difference between the largest eigenvalue and second largest, plotted in the y-axis, is the smallest for a value of  $\gamma N = 1 \implies \gamma = \frac{1}{N}$ , which will correspond to the maximum probability for the marked vertex, in optimal steps.

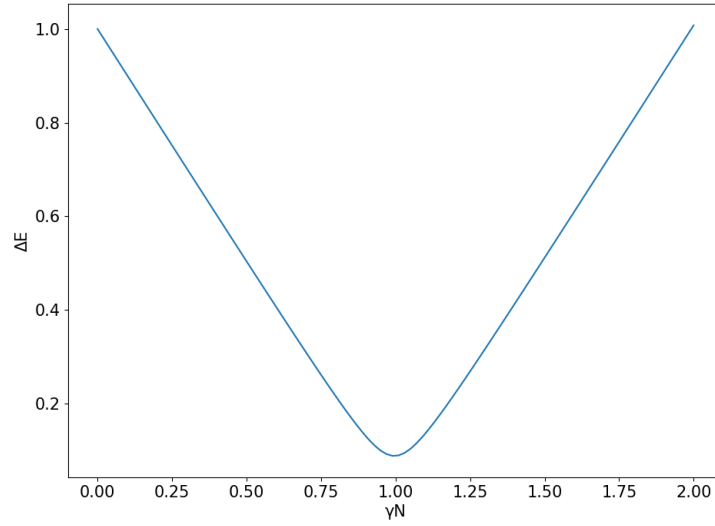


Figure 20: Value of the difference between the largest eigenvalue and the second largest, plotted as a function of  $\gamma N$ , for  $N = 512$ .

Figure 21 shows the evolution of the probability of the marked vertex in time, which is continuous in this model. In contrast with previous models, the distributions are smooth and reach exactly one, since the walk is allowed to evolve to exactly the ideal time steps.

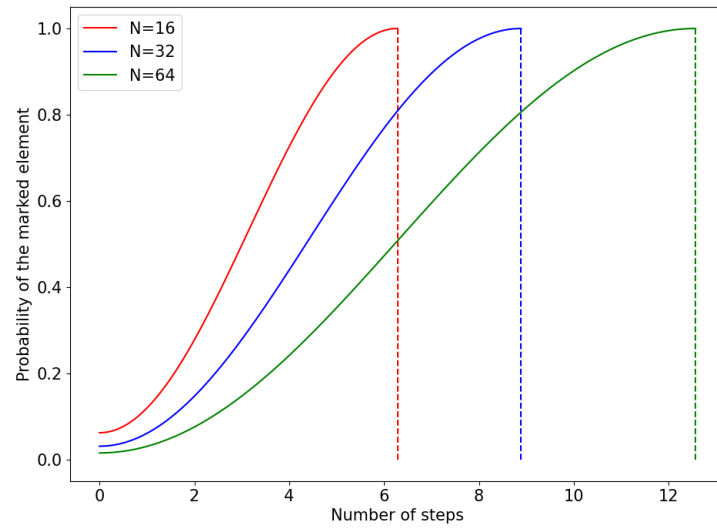


Figure 21: Continuous quantum walk search for a complete graph with 16, 32 and 64 vertices.

---

## IMPLEMENTATIONS AND APPLICATIONS

---

### 4.1 COINED

Consider the example of a quantum walker on a discretely numbered cycle. It was seen that the evolution operator associated with such a system is, as was defined in equation 37

$$U = S(C \otimes I), \quad (93)$$

where  $S$  is a shift operator, defined in equation 36 as

$$S = |0\rangle\langle 0| \otimes \sum_{x=-\infty}^{x=\infty} |x+1\rangle\langle x| + |1\rangle\langle 1| \otimes \sum_{x=-\infty}^{x=\infty} |x-1\rangle\langle x|, \quad (94)$$

that increments or decrements the position of the walker according to the coin operator  $C$ .

Previously, this system was simulated in Python by implenting it's equations. Now, the focus is to study a quantum circuit based on the work presented by [Douglas and Wang \(2009\)](#). This approach relies on multi-controlled CNOT gates in order to shift the state of the walker by  $+1$  or  $-1$ , each with a probability associated with the chosen coin, as can be seen in figure 22.

The generalized CNOT gates act on the node states as a cyclic permutator, where each node is mapped to an adjacent state. This can be seen as the walker moving left or right, in the uni-dimensional graph example.

The coin operator will simply be a Hadamard gate acting on a single qubit. For a graph with 16 nodes, for example, 4 qubits are required to encode each node and an extra qubit for the coin. The circuit will then be as shown in figure 23. Note that this circuit limits the number of graph nodes to powers of 2, and an arbitrary implementation of  $2^n$  nodes requires  $n + 1$  qubits. However, it is possible to have any number of nodes, given that the proper correction is made as can be seen in [Douglas and Wang \(2009\)](#). The method used was *Gray Code Ordering* proposed by [Slepoy \(2006\)](#), whereby a certain arrangement of CNOT gates results in control states only differing by a single bit.

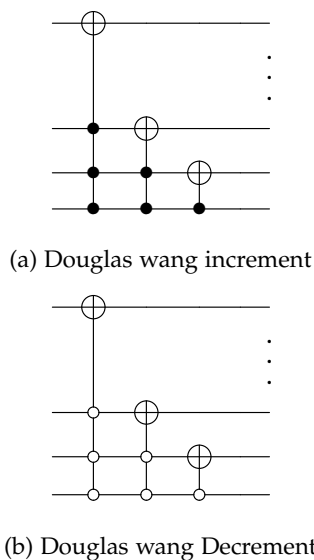


Figure 22: Douglas wang shift operator

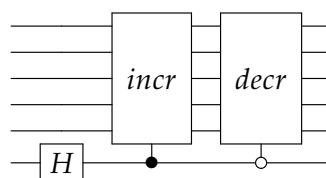


Figure 23: Douglas wang coined quantum walk circuit

In order to run this circuit on a real quantum computer using Qiskit, one must first find a way of creating generalized CNOT gates, since it is not available in the base package. One approach to this problem is to decompose an arbitrarily controlled CNOT gate into elementary gates, as was done by [Barenco et al. \(1995\)](#). In this context, the main idea is that for any unitary operator  $U$ , there exists operators such that

$$U = \phi A X B X C, \quad (95)$$

where  $ABC = I$ ,  $X$  is the Pauli- $X$  and  $\phi$  is a phase operator described by  $\phi = e^{i\delta} \times I$ .

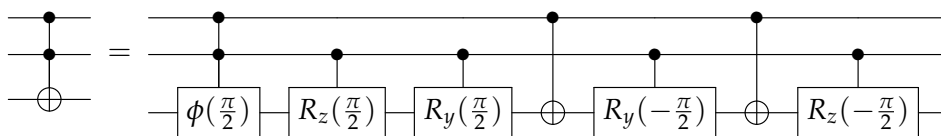


Figure 24: Toffoli decomposition

In order to understand this method, a good first example is the Toffoli gate, as is shown in figure 24. The first rotation in the circuit is defined by the  $R_z$  matrix

$$R_z(\theta) = \begin{pmatrix} e^{i\frac{\theta}{2}} & 0 \\ 0 & e^{i\frac{\theta}{2}} \end{pmatrix}, \quad (96)$$

where  $\theta = \frac{\pi}{2}$ . Secondly, the  $R_y$  rotation is

$$R_y(\phi) = \begin{pmatrix} \cos(\frac{\phi}{2}) & -\sin(\frac{\phi}{2}) \\ \sin(\frac{\phi}{2}) & \cos(\frac{\phi}{2}) \end{pmatrix}, \quad (97)$$

and  $\phi = \frac{\pi}{2}$ . The following rotations are simply  $R_z^\dagger$  and  $R_y^\dagger$ . Lastly, the phase operator  $\phi$  is

$$\phi(\delta) = \begin{pmatrix} e^{i\delta} & 0 \\ 0 & e^{i\delta} \end{pmatrix} \quad (98)$$

where  $\delta = -\frac{\pi}{2}$ . This phase correction is considered because otherwise

$$R_z(\frac{\pi}{2})R_y(\frac{\pi}{2})XR_y(-\frac{\pi}{2})XR_z(-\frac{\pi}{2}) = \begin{pmatrix} 0 & -i \\ -i & 0 \end{pmatrix} \neq X. \quad (99)$$

Introducing the phase correction results in

$$\phi(\frac{\pi}{2}) \begin{pmatrix} 0 & -i \\ -i & 0 \end{pmatrix} = \begin{pmatrix} i & 0 \\ 0 & i \end{pmatrix} \begin{pmatrix} 0 & -i \\ -i & 0 \end{pmatrix} = \begin{pmatrix} 0 & 1 \\ 1 & 0 \end{pmatrix} = X \quad (100)$$

However, since this is a global phase, it won't be included since it has no effect on the result of the measurement.

A more generalized version of this method can be seen in figure 25. Each individual generalized CNOT gate in this circuit can be expanded as was done for the Toffoli gate example, stopping once the generalised inverter gates are simply Toffoli gates.

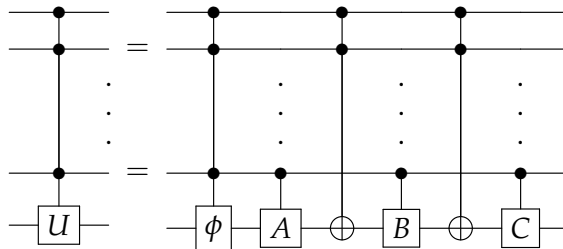


Figure 25: General decomposition

This was the chosen method because it provides a way of implementing arbitrarily controlled CNOT gates without the use of ancillary qubits, which are a scarce resource.

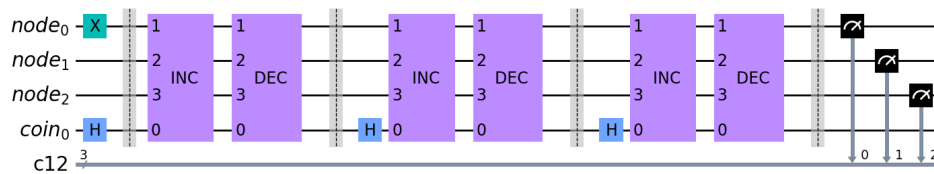


Figure 26: Temp

This circuit was implemented in Qiskit, as can be seen in figure 26. In this example, the increment and decrement sequence was applied three times on a graph of size  $2^3 = 8$  nodes. The starting position of the walker was set to  $\Psi(0) = |4\rangle$  and the Hadamard coin was used. The first block after the barrier is the sequence of operations that will increment the state of the walker, as is shown in figure 27. The circuit is simply the CNOT decomposition of figure 25 applied to the increment circuit of figure 22a for the  $N = 4$ , qubit case. The following

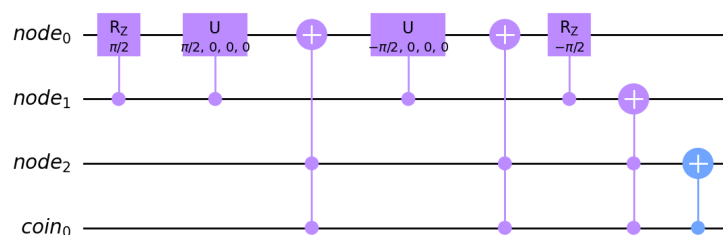


Figure 27: Temp

block represents the decrement of the state of the walker, which is just an increment block with it's controls negated as is shown in figure 28. The rest of the circuit is just the repetition of these operations as a function of the number of time steps required.



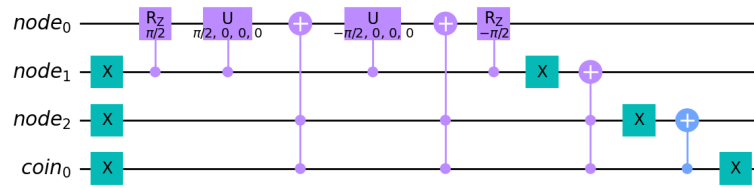


Figure 28: Temp

Lastly, the circuit is measured and the results can be seen in figure 29. These results can be verified by calculating the time evolution of the wave function associated with the system

$$|\Psi(0)\rangle = |4\rangle \quad (101)$$

$$|\Psi(1)\rangle = \frac{|0\rangle |x=3\rangle + |1\rangle |x=5\rangle}{\sqrt{2}} \quad (102)$$

$$|\Psi(2)\rangle = \frac{|0\rangle |x=2\rangle + |1\rangle |x=4\rangle + |0\rangle |x=4\rangle - |1\rangle |x=6\rangle}{2} \quad (103)$$

$$|\Psi(3)\rangle = \frac{|1\rangle |x=1\rangle - |0\rangle |x=3\rangle + 2(|0\rangle + |1\rangle) |x=5\rangle + |0\rangle |x=7\rangle}{2\sqrt{2}}. \quad (104)$$

Taking the modulus squared of the amplitudes associated with the states, confirms that the probability distribution presented in figure 29 is correct.

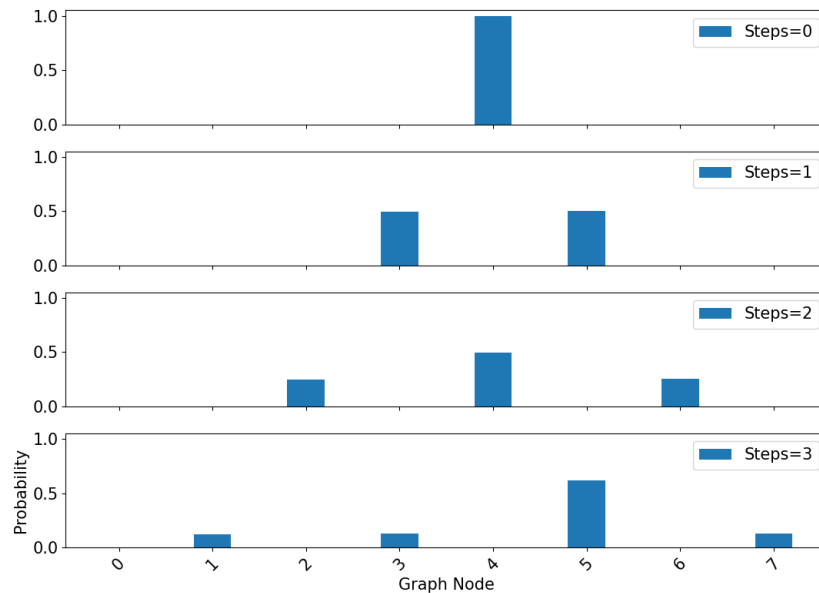


Figure 29: Temp

## 4.2 CONTINUOUS

As was seen in section 3.3, the unitary evolution operator of this model is defined as

$$U(t) = e^{-iHt} = e^{i(-\gamma L)t} = e^{-i\gamma(A+D)t}. \quad (105)$$

Considering a regular graph, this operator can be rewritten as

$$U(t) = \phi(t)e^{-i\gamma(A)t}, \quad (106)$$

where  $\phi(t)$  is a global phase and  $A$  is the adjacency matrix associated with the graph.

Here, the study will focus on the circuit implementation of this walk in a cyclic graph, and a different approach was used to define the adjacency matrix. This approach relies on the concept of a circulant graph, which are a class of graphs defined by a circulant matrix such that

$$A = \begin{pmatrix} c_0 & c_{N-1} & \cdots & c_3 & c_2 \\ c_1 & c_0 & c_{N-1} & & c_3 \\ \vdots & c_1 & c_0 & \ddots & \vdots \\ c_{N-2} & & \ddots & \ddots & c_{N-1} \\ c_{N-1} & c_{N-2} & \cdots & c_1 & c_0 \end{pmatrix}. \quad (107)$$

In order to generate the proper circulant graphs, restrictions on this matrix are needed. Firstly,  $c_0 = 0$ , since self-loops are not part of the structure. Secondly, the matrix must be symmetric, therefore  $c_{n-j} = c_j$ .

These matrices can be fully described by the first column of the matrix

$$v_1 = [c_0, c_1, \dots, c_{N-2}, c_{N-1}]^T \quad (108)$$

with a discrete convolution operator performing cyclic permutations of  $c$ , on each column. For example,

$$Dv_1 = [c_{N-1}, c_0, \dots, c_{N-3}, c_{N-2}]^T = v_2. \quad (109)$$

More specifically, for the cycle case

$$Dv_1 = D[0, 1, 0, \dots, 0, 1]^T = [1, 0, 1, 0, \dots, 0, 0]^T = v_2. \quad (110)$$

The operator can then be recursively defined as

$$Dv_k = v_{k+1}. \quad (111)$$

and the matrix will be

$$A = \sum_{j=0}^{N-1} Dv_j \quad (112)$$

$$A^k = \sum_{j=0}^{N-1} c_{(j-1) \bmod N} \quad (113)$$

The eigenvalues of a circulant matrix can be found by

$$\lambda_p = c_0 + \sum_{q=1} c_{N-q} \omega^{pq}, \quad (114)$$

and the eigenvectors are

$$|\varphi_p\rangle = \frac{1}{\sqrt{n}} \sum_{q=0}^{n-1} \omega^{pq}. \quad (115)$$

This given, it is possible to construct an operator that diagonalizes the circulant matrix through the eigenvectors, which is useful for constructing the circuit. For this purpous, the Quantum Fourier Transform can be used and it is defined as

$$F = \frac{1}{\sqrt{N}} \sum_{p,q} \omega^{pq} |p\rangle \langle q|. \quad (116)$$

The adjacency matrix of a circulant graph can then be diagonalized such that

$$A = F^\dagger \Lambda F, \quad (117)$$

where  $\Lambda$  is a diagonal operator that encodes the eigenvalues

$$\Lambda = \sum_j \lambda_j |j\rangle \langle j|. \quad (118)$$

The unitary operator of the walk can then be rewritten as

$$U = F^\dagger e^{i\gamma\Lambda t} F \quad (119)$$

where

$$e^{i\gamma\Lambda t} = \sum_j e^{i\gamma\lambda_j t} |j\rangle \langle j|. \quad (120)$$

The circuit can now be constructed making use of the *diagonal* function provided by Qiskit, which decomposes diagonal operators based on the method presented in theorem 7 of Shende et al. (2006). The other tool used was the Quantum Fourier Transform, also provided by the Qiskit package. Figure 30 shows the implementation of the circuit for 3 qubits or  $2^3 = 8$  graph nodes and  $t = 3$ .

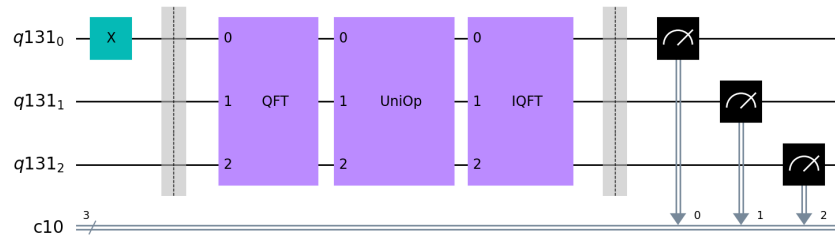


Figure 30: Temp

The circuit for the Quantum Fourier transform is well known and presented in figure 31. The circuit associated with  $F^\dagger$  is similarly constructed by negating the previous figure's rotations.

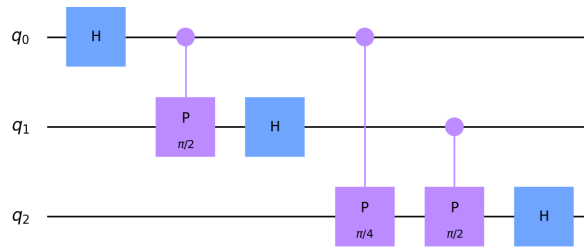


Figure 31: Temp

The circuit associated with the diagonal operator is show in figure 32. Furthermore equation 119 says that time is simply a constant inside the exponential, which means that the diagonal operator's circuit will not need extra gates when increasing time, it will only need different rotations and differ in global phase. This is an advantage when comparing to

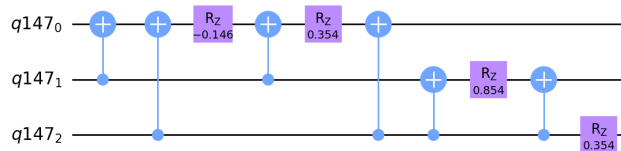


Figure 32: temp

the previous model, seen in figure 26, where each extra step required another increment

and decrement gates. Further evidence of this behaviour can be seen in figure 33, where it was created a circuit for  $t = 0$  up to  $t = 100$  with increments of 1. It was then counted the number of gates, for each circuit, and plotted against the respective time. This graph

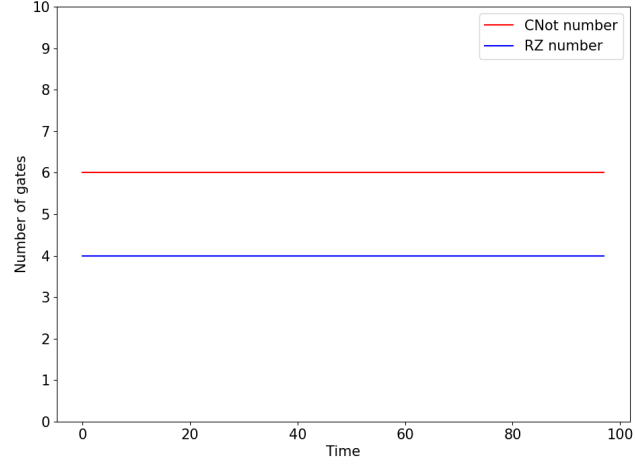


Figure 33: Temp

clearly shows that both the number of  $R_z$  rotations and CNot operations remain constant throughout the entire time interval.

Finally, the circuit was measured, and the result can be seen in figure 34

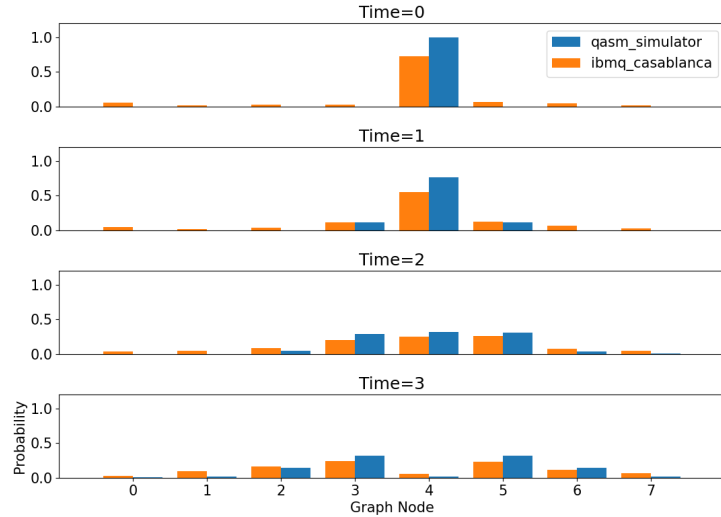


Figure 34: Temp

## 4.3 STAGGERED

## 4.4 SEARCH PROBLEMS WITH QISKIT

## 4.4.1 Grover

Like it was seen in section 2.1, Grover's algorithm is a quantum alternative to unstructured search problems. Consider the case of finding element  $x_0$  out of an unordered list of size  $N$ . Worst case scenario, a classical algorithm would need to check every element of the list, requiring  $N$  steps.

The first stage of Grover's algorithm is to create an uniform superposition of all states in the system

$$|\Psi_0\rangle = \frac{1}{\sqrt{N}} \sum_{x=0}^{N-1} |x\rangle. \quad (121)$$

Next is the application of the Grover iteration process, which starts with an oracle that adds a negative phase to the solution states

$$\mathcal{O} |x\rangle = (-1)^{f(x)} |x\rangle. \quad (122)$$

This operator can be seen as an identity matrix with negative entries corresponding to the solution states, and the operator can be rewritten as

$$\mathcal{O} = I - 2 \sum_{m \in M} |m\rangle \langle m|. \quad (123)$$

where  $I$  is the identity matrix and  $M$  is a set of solutions where  $f(m) = 1$ , otherwise it's 0. The matrix associated with this operator will be

$$\mathcal{O} = \begin{pmatrix} (-1)^{f(0)} & 0 & \dots & 0 \\ 0 & (-1)^{f(1)} & \dots & 0 \\ \vdots & 0 & \ddots & \vdots \\ 0 & 0 & \dots & (-1)^{f(N-1)} \end{pmatrix}. \quad (124)$$

The second part of the iteration is an amplitude amplification process by means of the diffusion operator

$$\mathcal{D} = (2 |\Psi_0\rangle \langle \Psi_0| - I) = H^{\otimes n} (2 |0\rangle \langle 0| - I) H^{\otimes n}. \quad (125)$$

The unitary operator that describes the Grover iteration process will then be

$$\mathcal{U} = \mathcal{D}\mathcal{O}. \quad (126)$$

As was shown in section 2.1 this iteration process will be done several times, depending on the number of elements. Optimal probability of success finding a single solution will be reached after  $\lfloor \frac{\pi}{4} \sqrt{N} \rfloor$  steps, and  $\lfloor \frac{\pi}{4} \sqrt{\frac{N}{K}} \rfloor$  for  $K$  solutions, which is a quadratic gain when compared to the classical case.

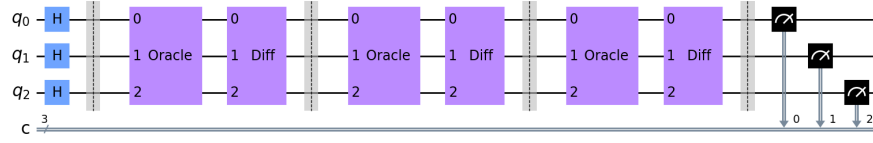


Figure 35: Temp

Consider the 3 qubit case, where  $N = 8$  and solution state  $|4\rangle$ . The optimal number of iterations is approximately 2, and figure 35 is the circuit for 3 iterations. The system starts with the creation of an uniform superposition state, which means applying Hadamard gates to each qubit. Immediately following the barrier, the first operator of the iteration process is

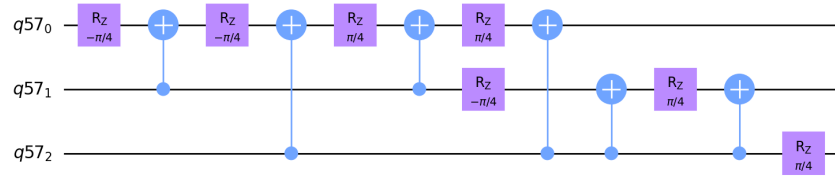


Figure 36: Temp

the oracle, which is shown in figure 36. Because the oracle operator is simply the identity matrix with negative entries corresponding to the solution states, it can be simply translated into a circuit by means of the diagonal function in Qiskit. The last part of the iteration is the diffusion operator, whose circuit is shown in figure 37.

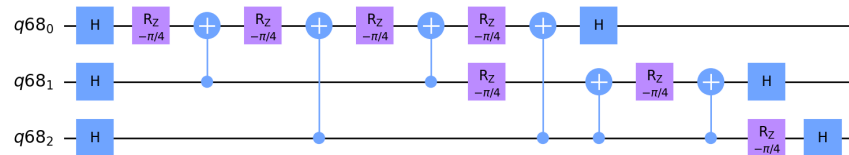


Figure 37: Temp

Comparing equations 123 and 125, it is easy to see why figures 36 and 37 are very similar. The diffusion circuit will simply be the oracle circuit for state  $|0\rangle$  in between Hadamard operations.

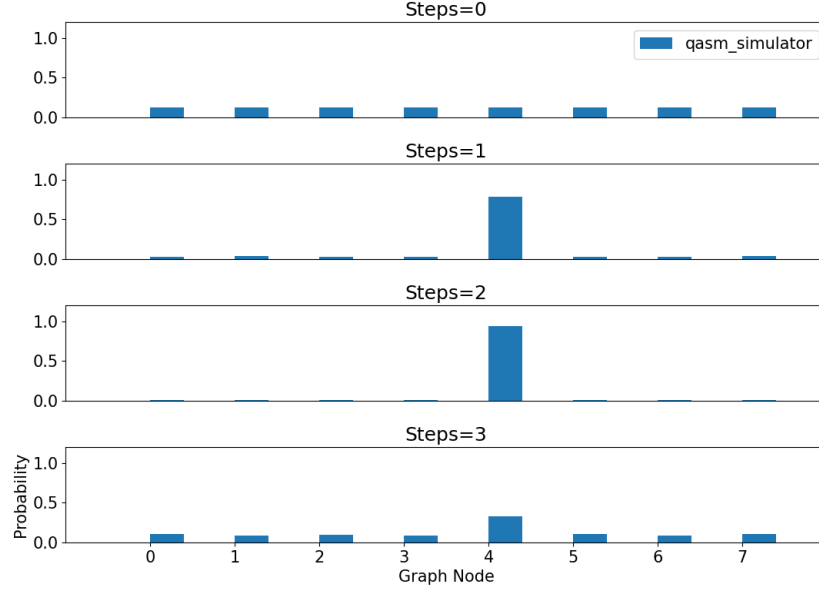


Figure 38: Temp

The results of measurement are shown in figure 38. As was expected, maximum probability for the marked element was reached after 2 iterations and it decreases in subsequent steps.

#### 4.4.2 Coined

As previously done in section 3.5.1, this chapter aims to expand the coined quantum walk model incorporating concepts like the oracle and diffusion operator of the Grover algorithm. In fact, for the complete graph case, the coined quantum walk and Grover's algorithm are equivalent.

The modified unitary evolution operator is

$$U' = S(\mathcal{O} \otimes G), \quad (127)$$

as was defined in equation 79, where  $S$  is the flip-flop shift operator,  $\mathcal{O}$  is the oracle operator and  $G$  is the Grover diffusion as a coin operator.

Consider the case of a complete graph, where every vertex is adjacent to one another. The quantum circuit to implement this, as shown in figure 39, will require  $N$  qubits to represent the state of the walker and  $N$  qubits for the state of the coin. The shift operator



was constructed based on the work of [Douglas and Wang \(2009\)](#), where the state of the walker is flip-flopped with the state of the coin, which can be done through swap gates.

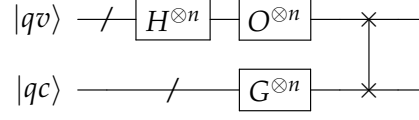


Figure 39: Douglas wang coined quantum walk circuit

This was implemented in Qiskit, for a graph of size  $N = 2^3 = 8$ , which means 6 qubits will be required. For the case of one marked element, the number of iterations that maximizes the amplitude of the solution state is  $\lfloor \frac{\pi}{2} \sqrt{N} \rfloor$ , and figure 40 shows the circuit for 5 iterations of the walk.

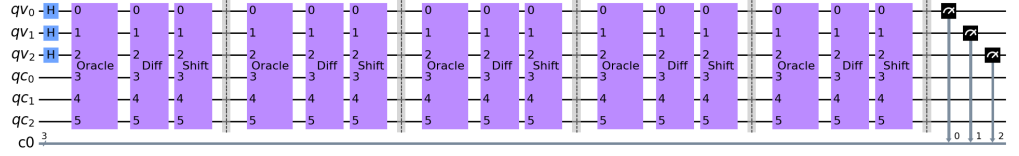


Figure 40: Temp

The circuit starts in a uniform superposition of the states corresponding to the vertices of the graph, and the first step of the iteration is the oracle. This operator will flip the amplitude of the vertex state  $|4\rangle$ , as is shown in figure 41. It is the same operator as in figure 36, but applied only to states belonging in the position space of the walk.

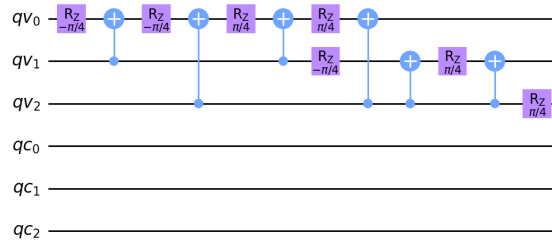


Figure 41: Temp

The states associated with the coin space of the walk will be transformed according to Grover's diffusion, as is seen in figure 42.

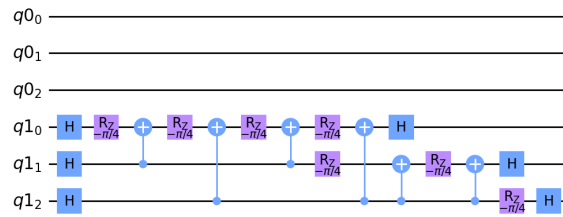


Figure 42: Temp

The final part of the iteration is the shift operator, as can be seen in figure 43. The flip-flop shift operator was defined in equation 74 as

$$S |v1\rangle |v2\rangle = |v2\rangle |v1\rangle, \quad (128)$$

where  $|v1\rangle$  represents the position of the walker and  $|v2\rangle$  is the state of the coin. It is trivial to implement this as shift operations between the vertex states and coin states.

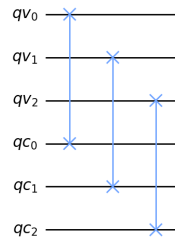


Figure 43: Temp

Lastly, measurements were performed, and the results plotted in figure 44. Maximum probability of the marked element was reached after 4 steps, and extra steps reduce said probability.

### 4.4.3 Continuous

As was seen in section 3.5.3, the unitary operator associated with the continuous time quantum walk model can be modified as to mark an element for amplitude amplification

$$U'(t) = e^{iH't} = \phi(t)e^{-i\gamma(A+O)t}, \quad (129)$$

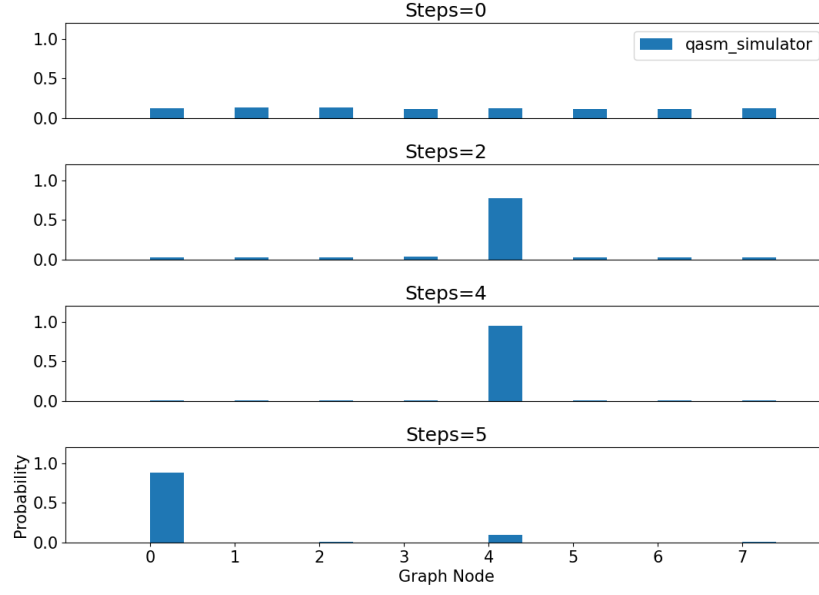


Figure 44: Temp

where  $\phi(t)$  is a global phase,  $A$  is the adjacency matrix and the oracle is defined as

$$O = \sum_{m \in M} |m\rangle \langle m|, \quad (130)$$

where  $M$  is the set of marked elements.

This section will focus on constructing and analyzing the circuit form of the continuous-time quantum walk search problem, and the first step is to borrow the diagonal definition of the adjacency matrix from equation 117

$$A = F^\dagger \Lambda F, \quad (131)$$

and use the Suzuki-Trotter expansion

$$e^{i(H_0+H_1)t} = \lim_{n \rightarrow \infty} (e^{i\frac{H_0t}{n}} e^{i\frac{H_1t}{n}})^n, \quad (132)$$

to decompose the operator in equation 129

$$e^{i\gamma(A+O)t} = \lim_{n \rightarrow \infty} (F^\dagger e^{i\gamma\frac{\Lambda t}{n}} F e^{i\gamma\frac{O t}{n}})^n, \quad (133)$$

which can be easily translated into circuit form as in figure 45.

Consider the case of a graph of size  $N = 3$  and trotter number of  $n = 2$ . The corresponding Qiskit circuit is as shown in figure 45. The system starts out in an uniform superposition followed by a state transformation according to the oracle operator that can be seen in figure

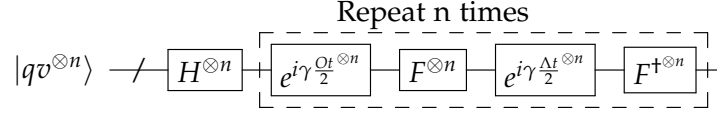


Figure 45: Temp

47. Note that the circuit was obtained by using the Qiskit diagonal function that takes the diagonal entries of the operator corresponding to the oracle, as in equation 133. The

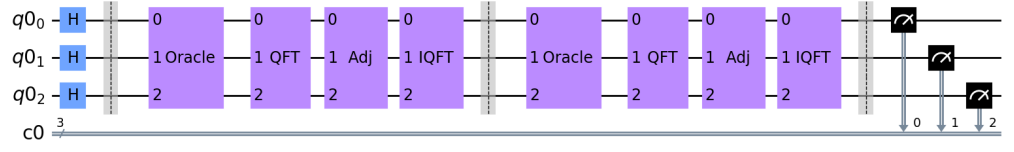


Figure 46: Temp

following transformations will be the quantum Fourier transform, which is the same as in figure 31, and the operator associated with the adjacency matrix. Since  $A$  is the diagonal adjacency matrix of a complete graph, it is easily implemented using Qiskit, as can be seen in figure 48.

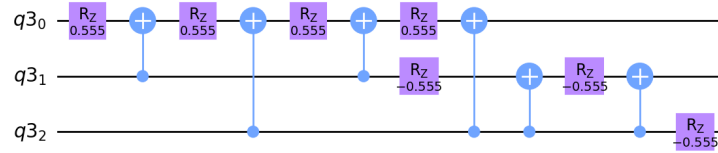


Figure 47: Temp

The results of measurement are shown in figure 49.

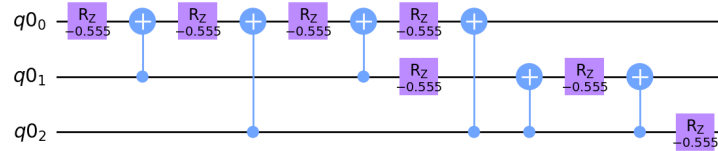


Figure 48: Temp

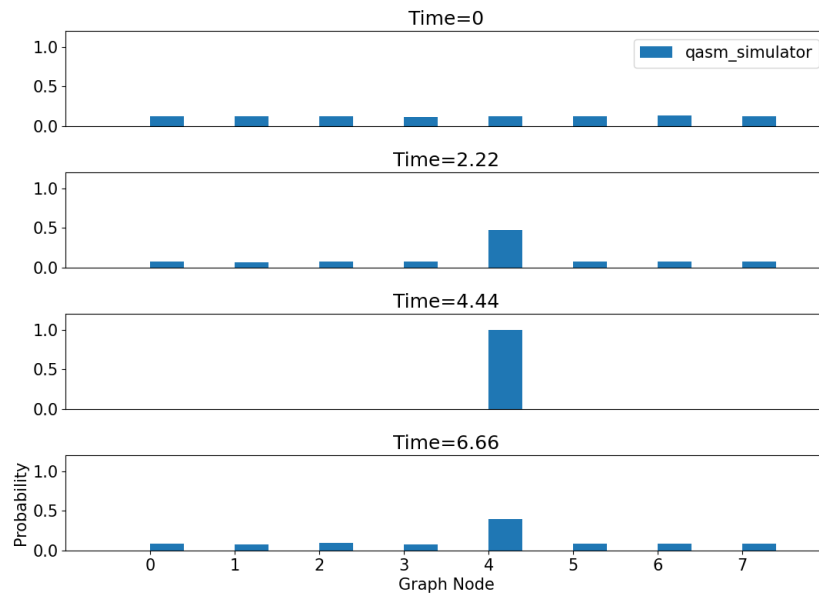


Figure 49: Temp

#### 4.4.4 Staggered

---

## DISCUSSIONS AND CONCLUSION

---

### 5.1 CONCLUSIONS

### 5.2 PROSPECT FOR FUTURE WORK

---

## BIBLIOGRAPHY

---

- Proceedings of the Royal Society of London. Series A: Mathematical, Physical and Engineering Sciences*, 452(1954):2551–2577, Nov 1996. ISSN 1471-2946. doi: 10.1098/rspa.1996.0136. URL <http://dx.doi.org/10.1098/rspa.1996.0136>.
- Andris Ambainis. Quantum walk algorithm for element distinctness. *SIAM Journal on Computing*, 37(1):210–239, 2007.
- Adriano Barenco, Charles H. Bennett, Richard Cleve, David P. DiVincenzo, Norman Margolus, Peter Shor, Tycho Sleator, John A. Smolin, and Harald Weinfurter. Elementary gates for quantum computation. *Physical Review A*, 52(5):3457–3467, Nov 1995. ISSN 1094-1622. doi: 10.1103/physreva.52.3457. URL <http://dx.doi.org/10.1103/PhysRevA.52.3457>.
- Adriano Barenco, Artur Ekert, Kalle-Antti Suominen, and Päivi Törmä. Approximate quantum fourier transform and decoherence. *Physical Review A*, 54(1):139–146, Jul 1996. ISSN 1094-1622. doi: 10.1103/physreva.54.139. URL <http://dx.doi.org/10.1103/PhysRevA.54.139>.
- Paul Benioff. The computer as a physical system: A microscopic quantum mechanical hamiltonian model of computers as represented by turing machines. *Journal of Statistical Physics*, 22(5):563–591, 1980.
- Charles Bennett and Gilles Brassard. Withdrawn: Quantum cryptography: Public key distribution and coin tossing. *Theoretical Computer Science - TCS*, 560:175–179, 01 1984. doi: 10.1016/j.tcs.2011.08.039.
- Charles H. Bennett and Stephen J. Wiesner. Communication via one- and two-particle operators on einstein-podolsky-rosen states. *Phys. Rev. Lett.*, 69:2881–2884, Nov 1992. doi: 10.1103/PhysRevLett.69.2881. URL <https://link.aps.org/doi/10.1103/PhysRevLett.69.2881>.
- Michael Boyer, Gilles Brassard, Peter Høyer, and Alain Tapp. Tight bounds on quantum searching. *Fortschritte der Physik*, 46(4-5):493–505, 1998.
- A. R. Calderbank and Peter W. Shor. Good quantum error-correcting codes exist. *Phys. Rev. A*, 54:1098–1105, Aug 1996. doi: 10.1103/PhysRevA.54.1098. URL <https://link.aps.org/doi/10.1103/PhysRevA.54.1098>.
- D. Cheung. Improved bounds for the approximate qft. 2004.

- Andrew M. Childs and Jeffrey Goldstone. Spatial search by quantum walk. *Physical Review A*, 70(2):022314, 2004.
- Andrew M. Childs, Richard Cleve, Enrico Deotto, Edward Farhi, Sam Gutmann, and Daniel A. Spielman. Exponential algorithmic speedup by quantum walk. *Proc. 35th ACM Symposium on Theory of Computing (STOC 2003)*, pp. 59-68, 2002. doi: 10.1145/780542.780552.
- D. Coppersmith. An approximate fourier transform quantum fourier transform useful in quantum factoring", ibm research report rc19642, r. cle. 1994.
- David Deutsch. Quantum theory, the church-turing principle and the universal quantum computer. *Proceedings of The Royal Society A Mathematical Physical and Engineering Sciences*, 400(1818), 1985.
- David Deutsch and Richard Jozsa. Rapid solution of problems by quantum computation. *Proceedings of The Royal Society A Mathematical Physical and Engineering Sciences*, 439(1907), 1992.
- B.L. Douglas and J. B. Wang. Efficient quantum circuit implementation of quantum walks. 2009.
- Richard P. Feynman. There's plenty of room at the bottom. *Feynman and computation*, pages 63-76, 1959.
- Richard P. Feynman. Simulating physics with computers. *International Journal of Theoretical Physics*, 21(6-7):467-488, 1982.
- Steven Finch. "pólya's random walk constant." in mathematical constants. *Cambridge University Press*, pages 322-331, 2003.
- Lov K. Grover. A fast quantum mechanical algorithm for database search. *STOC '96 Proceedings of the twenty-eighth annual ACM symposium on Theory of computing*, pages 212-219, 1996.
- Elliott Montroll. Random walks in multidimensional spaces, especially on periodic lattices. *Journal of the Society for Industrial and Applied Mathematics*, 4(4):241-260, 1956. doi: 10.1137/0104014.
- Elliott Waters Montroll and George Herbert Weiss. Random walks on lattices. ii. *Journal of Mathematical Physics*, page 167-181, 1997.
- Gordon E. Moore. Cramming more components onto integrated circuits. *Electronics*, 38(8): 114-117, 1965.



- Karl Pearson. The problem of the random walk. *Nature*, 72(1865):294, 1905. doi: 10.1038/072294bo.
- J. Pollard, Lenstra Arjen, H. Lenstra, and Mark Manasse. The number field sieve. 1994.
- Renato Portugal. *Quantum Walks and Search Algorithms*. Springer, 2018.
- Renato Portugal, M. C. de Oliveira, and J. K. Moqadam. Staggered quantum walks with hamiltonians. *Physical Review A*, 95(1):012328, 2017.
- George Pólya. Über eine aufgabe der wahrscheinlichkeitsrechnung betreffend die irrfahrt im straßennetz. *Mathematische Annalen*, 84:149–160, 1921. doi: 10.1007/BF01458701.
- Benjamin Schumacher. Quantum coding. *Phys. Rev. A*, 51:2738–2747, Apr 1995. doi: 10.1103/PhysRevA.51.2738. URL <https://link.aps.org/doi/10.1103/PhysRevA.51.2738>.
- C. E. Shannon. A mathematical theory of communication. *The Bell System Technical Journal*, 27(3):379–423, 1948. doi: 10.1002/j.1538-7305.1948.tb01338.x.
- V.V. Shende, S.S. Bullock, and I.L. Markov. Synthesis of quantum-logic circuits. *IEEE Transactions on Computer-Aided Design of Integrated Circuits and Systems*, 25(6):1000–1010, Jun 2006. ISSN 1937-4151. doi: 10.1109/tcad.2005.855930. URL <http://dx.doi.org/10.1109/TCAD.2005.855930>.
- Peter W. Shor. Algorithms for quantum computation: Discrete logarithms and factoring. *Proceedings 35th Annual Symposium on Foundations of Computer Science*, pages 124–134, 1994a.
- P.W. Shor. Algorithms for quantum computation: discrete logarithms and factoring. *Proceedings 35th Annual Symposium on Foundations of Computer Science*, pages 124–134, 1994b. doi: 10.1109/SFCS.1994.365700.
- Alexander Slepoy. Quantum gate decomposition algorithms. *Sandia National Laboratories*, 2006.
- Tommi Sottinen. Fractional brownian motion, random walks and binary market models. *Finance and Stochastics*, (5):343–355, 2001. doi: 10.1007/PL00013536.
- Alan Turing. On computable numbers, with an application to the entscheidungsproblem. *Proceedings of the London Mathematical Society*, s2-42(1):230–265, 1936.
- Salvador Elías Venegas-Andraca. Quantum walks: a comprehensive review. *Quantum Information Processing*, 11(5):1015–1106, 2012.
- J. von Neumann. First draft of a report on the edvac. *IEEE Annals of the History of Computing*, 15(4):27–75, 1993. doi: 10.1109/85.238389.

Stephen Wiesner. Conjugate coding. *SIGACT News*, 15(1):78–88, 1983. ISSN 0163-5700. doi: 10.1145/1008908.1008920. URL <https://doi.org/10.1145/1008908.1008920>.

Christof Zalka. Grover’s quantum searching algorithm is optimal. *Physical Review A*, 60(4): 2746–2751, 1999.



---

## SUPPORT MATERIAL

---